Crystal cargo perspectives on magma assembly and dynamics during the 2021 Tajogaite eruption, La Palma, Canary Islands

Manuscript submitted to Volcanica Dec 2024; Accepted version 24/06/2025

Katy J. Chamberlain[1]*, Matthew J. Pankhurst[2,3,4], David A. Neave[5], Daniel J. Morgan[6], Olivia A. Barbee[7], Jane H. Scarrow[8], James Hickey[9], Sam Broom-Fendley[9], Joe Gardner[1], Gavyn K. Rollinson[9], Richard Walshaw[6], Alexander G. Stewart[5], Penny E. Wieser[10], Beverley C. Coldwell[2,3], Alba Martín-Lorenzo[2,3], and Fátima Rodríguez[2].

[1]Department of Earth, Ocean, and Ecological Sciences, School of Environmental Sciences, University of Liverpool, Liverpool, UK
[2]Instituto Volcanológico de Canarias (INVOLCAN); San Cristóbal de La Laguna, Tenerife, Spain
[3]Instituto Tecnológico y de Energías Renovables (ITER), Granadilla de Abona, Tenerife, Spain
[4]Now at: Gaiaxiom, Copenhagen, Denmark
[5]Department of Earth and Environmental Sciences, University of Manchester, Manchester, UK
[6]School of Earth and Environment, University of Leeds, Leeds, UK
[7]Xnovo Technology, Køge, Denmark
[8]Department of Mineralogy and Petrology, University of Granada, Granada, Spain
[9]Department of Earth and Environmental Sciences, University of Exeter, Penryn, UK
[10]Department of Earth and Planetary Science, University of California, Berkeley, CA, USA

* k.j.chamberlain@liverpool.ac.uk

ORCiD (KJC): 0000-0002-2010-6182
ORCiD (MJP): 0000-0001-6593-7740
ORCiD (DAN): 0000-0001-6343-2482
ORCiD (DJM): 0000-0002-7292-2536
ORCiD (OAB): 0000-0002-5618-2371
ORCiD (JHS): 0000-0001-8585-8679
ORCiD (JH): 0000-0002-5391-3415
ORCiD (SB-F): 0000-0001-7426-8657
ORCiD (JG): 0000-0002-8593-0201
ORCiD (GKR): 0000-0002-0655-6304
ORCiD (AGS): 0000-0002-4710-1963
ORCiD (PEW): 0000-0002-1070-8323
ORCiD (BCC): 0000-0001-9240-6240
ORCiD (AM-L): 0000-0001-8919-702X
ORCiD (FR): 0000-0003-4659-7810

Keywords: Tajogaite eruption; Canary Islands; petrological monitoring; Eruption dynamics

Abstract

The 2021 eruption of Tajogaite was the longest duration eruption, most voluminous, and had the largest human impact in recorded history on La Palma, Canary Islands. Extensive geophysical and geochemical data were collected during both the preceding unrest and eruptive event. Petrological monitoring was largely restricted to rapid stereo microscope observation and a few supporting in-depth studies using analytical instruments off-island. Here, we utilise time-series samples of lava and tephra from the Tajogaite eruption collected with near-daily frequency to understand the magmatic processes responsible for changes in petrological, geochemical, and geophysical observations. We combine published whole-rock major and trace element data with new QEMSCAN textural and mineral abundance data, major element analyses of the major macrocryst phases, and trace element data from clinopyroxene to illustrate magma plumbing system processes, supported by pressure and temperature modelling of mineral growth. Finally, we calculate olivine Fe-Mg diffusion timescales from early erupted tephra, and compare them with timescales of the climactic unrest period.

Our data indicate that more-evolved and mineralogically-diverse magmas were tapped during the first week of the eruption, with little evidence for magma mixing. Magma mixing only becomes apparent when more primitive magmas erupted after the first ~10 days, exemplified by reverse-zoned olivines. Nonetheless, clinopyroxene barometry suggests that much of the erupted material is fed from the upper mantle at all stages of the eruption. Timescales of this process overlap with, and extend, the record of climactic geophysical unrest, suggesting that destabilisation of the magma system started before geophysical methods alone could detect and resolve variations from background. The chemical compositions of the crystal cargo are surprisingly uniform from Stage 2 (~5 - 10 days of activity) to eruption cessation (after 85 days of activity), and changes in whole-rock and tephra glass compositions observed by previous studies are not obviously mirrored in the mineral record. We highlight the importance of combining both whole-rock and mineral scale observations to understand how eruptions progress, and ultimately end.

Second-language abstract

La erupción de Tajogaite de 2021 fue la de mayor duración, la más voluminosa y la de mayor impacto humano entre las erupciones históricas registradas en La Palma, Islas Canarias. Se recogieron numerosos datos geofísicos y geoquímicos tanto durante el periodo de inestabilidad previo como durante el evento eruptivo. El monitoreo petrológico consistió en gran medida en observaciones in situ con microscopio estereoscópico y en algunos estudios analíticos en profundidad realizados fuera de la isla. En este trabajo, utilizamos muestras de series temporales de lava y tefra de la erupción de Tajogaite, recogidas con una frecuencia casi diaria, para comprender los procesos magmáticos responsables de los cambios observados en los datos petrológicos, geoquímicos y geofísicos. Combinamos datos publicados de elementos mayores y traza en roca total con nuevos datos texturales y de abundancia mineral obtenidos mediante QEMSCAN, análisis de elementos mayores de las principales fases macrocristalinas, y datos de elementos traza en clinopiroxeno para ilustrar los procesos del sistema alimentación magmática, respaldados por modelos de presión y temperatura del crecimiento mineral. Finalmente, calculamos las escalas de tiempo de difusión de Fe-Mg en olivino a partir de tefra emitida en las primeras fases y las comparamos con las series temporales del periodo de mayor inestabilidad previo a la erupción.

Nuestros datos indican que, durante la primera semana de la erupción, se emitieron magmas más evolucionados y con mayor diversidad mineralógica, con escasa evidencia de mezcla magmática. La mezcla de magmas solo se hace evidente cuando los magmas más primitivos fueron emitidos después de los primeros ~10 días de erupción, lo que se ejemplifica mediante olivinos con zonación inversa. No obstante, la barometría en clinopiroxeno sugiere que gran parte del material emitido fue alimentado desde el manto superior en todas las etapas de la erupción. Las series temporales de este proceso se superponen con el periodo de mayor inestabilidad geofísica, e incluso se extienden, lo que sugiere que la desestabilización del sistema magmático comenzó antes de que los métodos geofísicos pudieran detectar y resolver variaciones respecto a valores de fondo. Las composiciones químicas de los cristales presentes en el magma son sorprendentemente uniformes desde la Etapa 2 (~5 - 10 días de actividad) hasta el final de la erupción (después de 85 días de actividad), y los cambios en la composición de la roca total y del vidrio de tefra observados por estudios previos no se reflejan claramente en el registro mineralógico. Destacamos la importancia de combinar observaciones tanto a escala de roca total como a escala mineral para comprender cómo progresan, y finalmente terminan, las erupciones.

Introduction

The societal impacts of long-lived (> few days) mafic eruptions are often significant, wide-ranging, and dynamic, despite appearing less catastrophic than historic large-scale (yet comparatively very short-lived) explosive felsic eruptions. With eruption longevity also comes the opportunity to better understand magma plumbing system dynamics because knowing when, and in what order, material exits a system, places important constraints upon petrogenetic models. To better mitigate the impacts of long-lived eruptions, we must understand how magma ascent pathways and the evolution of magmas might influence longevity and eruptive style. Yet, geophysical and geochemical signals (measurable prior to eruption initiation, and available in near real-time) can only reveal some magmatic processes through indirect observations of phenomena produced by magma ascent (e.g. changes in species and abundances of gas emissions, seismicity, ground deformation). In order to fully understand how magmas evolve (and thus the potential styles of eruption) both before and during eruptive episodes, geophysical and geochemical signals must be combined with petrological and geochemical assessments of erupted products, providing direct observations of magma ascent (Cassidy et al., 2018; Re et al., 2021). Petrology is hindered with respect to eruption forecasting, as it necessitates the eruption having begun to provide material to analyse. Yet the value in petrological study of volcanic products is highlighted when eruptive behaviour is prolonged, and has the potential to help understand how and when eruptions will end, another vital question during volcanic crises (e.g. Gansecki et al., 2019; Re et al., 2021; Bindeman et al., 2022; Corsaro et al., 2022; Halldórsson et al., 2022; Scarrow et al., 2024). Therefore, by coupling geophysical, geochemical and petrological studies of recent periods of volcanic activity, a more complete picture of how magmas assemble, ascend and erupt, and how eruptions are sustained and ultimately end may be achieved.

Ocean island provinces with high magma flux, such as Hawai'i, Iceland, and the Galápagos, are dominated by mafic eruption products and commonly experience extended periods of eruptive activity (e.g. Thordarson & Larsen, 2007; Poland et al., 2014; Bernard et a., 2019). For example, recent activity in 2021, 2022 and 2023 in Fagradalsfjall, Iceland, lasted for 184, 19 and 27 days respectively (Global Volcanism Programme, 2023). During these periods, whilst activity is typically effusive to only weakly explosive, it becomes important to forecast not just the start of eruptive activity, but also its end. These styles of eruptions typically present low risk to life, yet have extensive destructive effects on land use, and are costly to recover from. For example, the 2018 Kīlauea eruption triggered the evacuation of more than 3000 people, destroyed 723 buildings and recovery will cost >$800M USD (Houghton et al., 2021, Meredith et al., 2024). The Canary Islands are another example, of dominantly mafic, ocean island volcanoes but with a relatively low magmatic flux when compared with Hawai'i and others. They are a key natural laboratory to integrate across various sub-disciplines, having experienced multiple eruptions in historic times, including the 2021 Tajogaite eruption (e.g. Carracedo et al., 1998, 1999; Pankhurst et al., 2022; Bonadonna et al., 2022, Ubide et al., 2023, Longpré et al., 2025).

Petrological study of erupted products has the potential to deconvolve subsurface magmatic processes in the lead up to, and during, eruptive episodes, that can sometimes be masked when only considering whole-rock chemical compositions or geophysical and geochemical monitoring data (e.g. Corsaro & Miraglia, 2022; Weber et al., 2023). Crystals in volcanic products are scientifically valuable as they directly record dynamic magmatic processes that are otherwise inaccessible, and as such have been examined for decades, and in ever-increasing detail using a widening set of methods (e.g., Streck, 2008). Each crystal can be considered a microscale record of its own history experiencing local magmatic environments. Mineral compositions and textures can be used to infer pressures and temperatures of mineral growth/equilibria within magmatic plumbing systems (e.g. Barker et al., 2015; Halldórsson et al., 2018; Weber et al., 2024), interactions between different magma batches (e.g. Allen et al., 2013; Neave et al., 2014; Pizarro et al., 2019; Ruth & Costa, 2021) and the timescales over which these pre- and syn-eruptive processes occurred (e.g. Morgan et al., 2006; Chamberlain et al., 2014; Pankhurst et al., 2018; Conway et al., 2020; Kahl et al., 2022; Mangler et al., 2022; Ostorero et al., 2022). Yet, due to questions of how significant and representative each crystal's record might be, extrapolation to macro-scale processes is non-trivial. Hence most crystal-scale studies search for populations and patterns using as many crystals as feasible when attempting to understand something of the system as a whole. Far rarer are studies that place crystal-scale observations within the context of an ongoing/evolving eruption (e.g. Pankhurst et al., 2018, Matthews et al., 2024), where the significance they may hold and interpretations they are used to construct might be independently tested. It is these verifiable links formed between petrological observation (applied to the products of any eruption in the rock record), and direct observation of volcanic processes of the same eruption (which cannot be made restrospectively), that have the greatest promise to better understand volcanic eruptions. This linkage between the past rock record, and present-day monitoring of witnessed eruptions will allow us to both to interpret the past, as well as plan for the future.

In this paper we present a time series of mineral compositions, textures, intensive variables and timescales over the 85-day Tajogaite eruption on La Palma, in late 2021. By coupling mineral compositions, textures and modelled information (temperatures, pressures and timescales) to whole-rock compositions and observed geophysical signals, we highlight the advantages of detailed in situ mineral studies during eruptions. Additionally, we pinpoint the key analyses which could be prioritised in future periods of volcanic activity to better understand how eruptions progress. By integrating geophysical and geochemical insights into eruption progression, we can also refine the tuning of petrological monitoring of different systems (e.g. Re et al., 2021, Pankhurst et al., 2022).

Geological setting

La Palma is an intraplate volcanic island, and the most northwestern of the seven Canary Islands (Carracedo et al., 1998). The Canary Islands developed on Jurassic oceanic crust (Schminke et al., 1998), and weakly trend from oldest volcanic islands in the eastern sector of the island chain to younger volcanic islands in the western sector (Geldmacher et al., 2005), leading some authors to suggest a mantle plume origin for the archipelago (e.g. Hoernle et al., 1993). However, historic eruptions are distributed across the entire ~500 km east-west spread of islands, which argues against a simple hotspot-track model.

The volcanism that created La Palma began ~4 Ma with an initial seamount phase lasting for ~1 Myr (Staudigel et al., 1986; Carracedo et al., 1999). The first subaerial volcanism is preserved in the north of the island where the shield volcano of Taburiente, and subsequent edifices of Bejenado and Cumbre Nueva were active from ~1.7 Ma to ~410 ka (Fig. 1). The youngest, and historically active, edifice of Cumbre Vieja (125 ka to present) encompasses the southern section of La Palma (Barker et al., 2015; Day et al., 1999; Carracedo et al., 2001). Cumbre Vieja has produced eight historically recorded eruptions (Fig. 1), with vents aligned roughly north-south along, and below, the axial ridge of the Cumbre Vieja complex (Carracedo, 1994). The Cumbre Vieja complex is dominantly composed of silica-undersaturated alkaline mafic lava flows and scoria cones, with rare but evenly dispersed evolved plugs and flows (Klügel et al., 2006; Fig. 1). Cumbre Vieja rocks range from basanite/tephrite to phonolite; common mineral phases are clinopyroxene, olivine +/- titaniferous amphibole in mafic products, and amphibole + clinopyroxene + haüyne + apatite + plagioclase in more evolved magmas (Carracedo et al., 2001; Carracedo & Troll, 2016).

The 2021 eruption began on the 19th of September, lasted for 85 days (to 13th December) and produced the Tajogaite scoria cone complex, lava field, and tephra blanket. Prior to eruption initiation, unrest occurred periodically for ~4 years with deep (15 - 35 km) seismic swarms, and changes in gas emissions (Torres-González et al., 2020; Fernández et al., 2021; Padrón, 2022). In the week prior to eruption, intense and migrating seismic unrest and ground deformation occurred (Carracedo et al., 2022; Civico et al., 2022; Romero et al., 2022; Wadsworth et al., 2022). The eruption commenced explosively and sustained a tephra column, which developed into a NW-SE trending fire-fountaining fissure ~500 m long that fed lava flows. Up to six vents were active at various stages during the eruption, with NW vents more associated with lava flows and passive degassing, whereas SE vents were mostly associated with tephra plumes and lava fountains (Romero et al., 2022; Bonadonna et al., 2022). Strombolian activity resulted in a ~12 km^2 lava field being emplaced on the west side of the island, and ~2.3 x 10^7 m^3 of tephra being deposited over the island and sea (Bonadonna et al., 2022). As a result of the sustained eruption, more than 7,500 people were evacuated, and 2,800 buildings were destroyed or damaged (Bonadonna et al., 2022; Carracedo et al., 2022). Studies have already been undertaken on the geophysical (e.g. D'Auria et al., 2022; Piña-Varas et al., 2023; Suarez et al., 2023), geochemical (e.g. Day et al., 2022; González-Garcia et al., 2023; Ubide et al., 2023), and physical volcanology aspects of the eruption (e.g. Bonadonna et a., 2022; Tadeucci et al., 2023; Di Fiore et al., 2023), with a detailed time-series study of lava and tephra whole-rock compositions (Scarrow et al., 2024) highlighting three key phases within the eruption defined by correlated changes in magma compositions, geophysical observations, and eruptive phenomena.

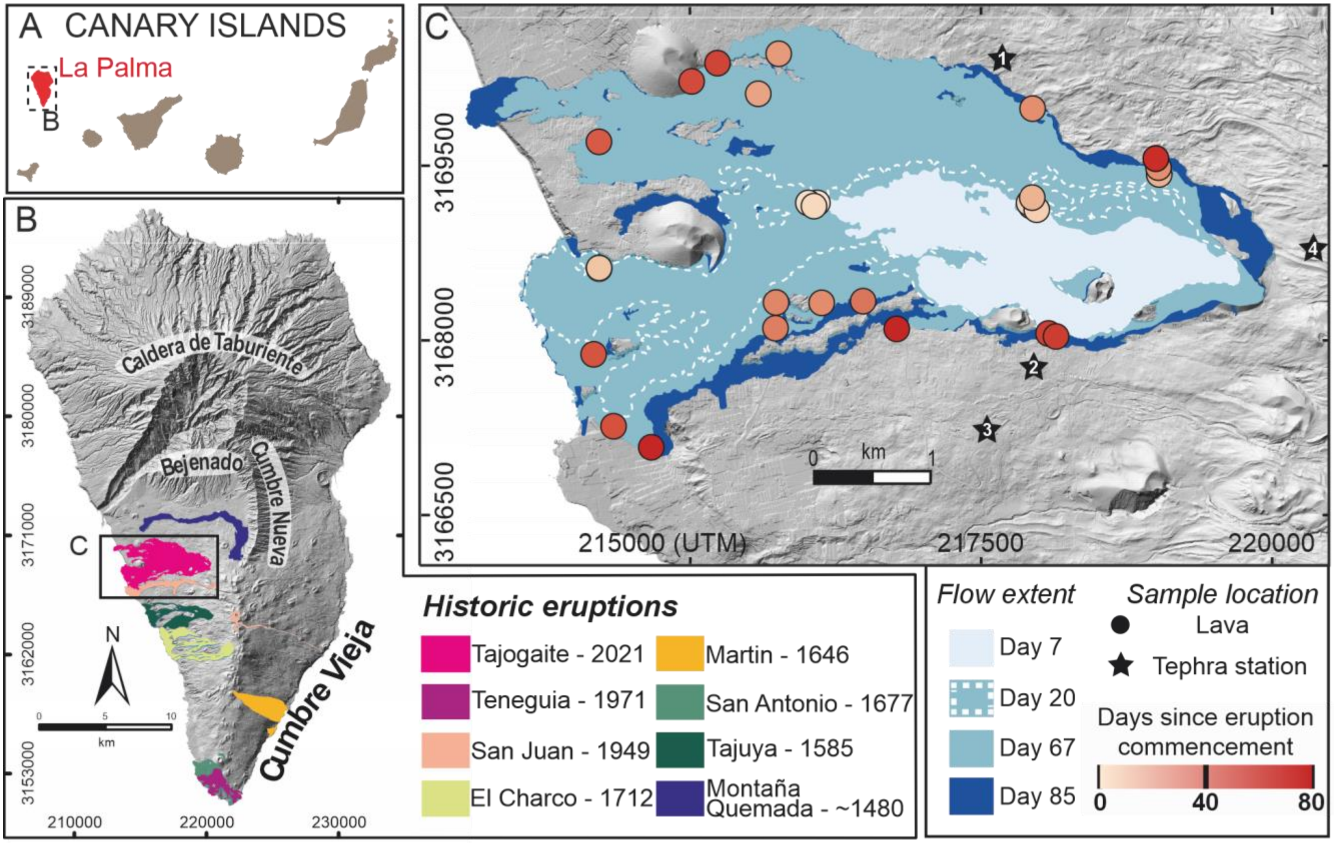

Figure 1: [A] Location of La Palma in the Canary Islands archipelago; [B] Location and extent of historic eruptions on La Palma showing the focus of activity along the Cumbre Vieja ridge. Tajogaite 2021 eruption: [C] Lava field extent by varying shades of blue; lava sample locations – circles, coloured by eruption date – and tephra collection pit locations – numbered black stars. Many sample sites were inundated by later flows. Modified from Scarrow et al. (2024).

Samples and methods

Following whole-rock analysis (see Scarrow et al., 2024), key samples were selected from across the entire duration of the eruptive sequence for textural and *in-situ* mineralogical analyses. Twenty-nine samples of lava, including the earliest and latest accessible erupted material, alongside five samples of tephra were selected for imaging and diffusion modelling (Table 1). Aliquots of samples were cut into thick sections at the Universidad de Granada, Spain, and polished to 0.25 microns for textural analysis.

Quantitative Evaluation of Materials by Scanning Electron Microscopy (QEMSCAN®) analysis of thick sections was undertaken at the Camborne School of Mines, University of Exeter, UK using a QEMSCAN® 4300 (Gottlieb et al., 2000). iMeasure v4.2SR1 and iDiscover 4.2SR1 and 4.3 (Rollinson et al., 2011) were used for sample measurement and data processing. The QEMSCAN® operated at 25 kV, 5 nA, a 1000 X-ray count rate per pixel, a working distance of around 22 mm under high vacuum and with beam calibration every 30 minutes. Sample measurement used the fieldscan measurement mode (Pirrie and Rollinson, 2011) to analyse the samples at an X-ray resolution/pixel spacing of either 5 or 10 microns and a 1000 micron^2 field size (x68 magnification). QEMSCAN® data were processed to produce a phase map and an olivine composition map per sample, in which each distinct phase/composition was assigned an 8-bit pixel intensity value. Olivine compositions were divided into 4 equal ranges of forsterite content (using the Fe-Mg ratio in the raw data) which were later calibrated using Electron Probe Microanalysis (EPMA) data (see next paragraph). Pixels that did not fit the strict raw data requirements needed to be assigned a mineral phase were assigned to "Undifferentiated groundmass", and instead reflect pixels containing glass or a combination of minerals ± glass below the pixel resolution. Isolated pixels of chemically complex phases may be the result of partial- or sub-volume interaction and not a true representation of phase abundance. Isolated and small clusters of QEMSCAN® pixels of amphibole were shown by back-scatter electron (BSE) data to be particularly prone to these effects, and so were added to the groundmass. Individual phase maps were extracted, labelled and analysed in *Python* using the pandas, numpy, and skimage libraries. We chose an area of 10,000 microns^2 to reflect the minimum size of macrocrysts, and assigned every region smaller than this limit to the groundmass. Pixel connectivity was determined as any of 4 neighbours, as opposed to 8 neighbours (any adjacent pixel including on the corners), which was found to be more accurate in delineating groundmass crystals from each other and so minimising clusters of groundmass crystals being assigned to the macrocryst classification. We estimate the abundance of macrocrysts to be accurate within 5%, as the styles of groundmass crystal clustering from phase to phase, and watershed parameters needed to separate them generate slightly differing results. An exhaustive methodological description is outside the scope of this work because, for our purposes of tracking possible changes across the eruption, any changes in data reduction method (which is applied to all samples at the same time) do not change the trends or interpretation. Phases that contributed ≥5% macrocrysts by area (all area values are normalised to solid rock area) in at least one sample were categorised as "major", while the rest were categorised as "minor". Full details of the QEMSCAN® methodology can be found in Electronic Appendix 1.

Following QEMSCAN® analysis, key mineral species (olivine, clinopyroxene, amphibole) were identified and major element analyses were obtained by EPMA using a JEOL JXA 8230 instrument at the University of Leeds, using wavelength-dispersive spectrometry. Analytical conditions varied depending on the phase being analysed. Tephra matrix glass major and minor element concentrations were analysed from five key samples spanning eruptive days 3 - 80+, only totals between 98 and 102 wt.% were accepted as reliable, and normalised to 100 wt.% for comparison with existing glass data. For full details of conditions and precision and accuracy of EPMA data see Electronic Appendix 2.

Olivine EPMA spots were co-located in the QEMSCAN® data and used to build a 38-point calibration (see Electronic Appendix 1) that returns a R^2 value of 0.98 from a linear regression. This calibration provides compositional quantification of the olivine distribution using the much larger QEMSCAN® dataset. The spots used for calibration were selected to span a range of Fo values (78.6 - 84.7 from a full dataset range of 78.1-85.9) and located within homogeneous core regions of olivine as observed from image analysis of QEMSCAN® and BSE images (see Pankhurst et al. 2018 and Pankhurst et al. 2019 for EPMA-BSE calibration methods). QEMSCAN pixel values from these regions were measured using ImageJ, where 1 is the most forsteritic range and 4 the most fayalitic, and the averaged values' standard error of the mean provides a measure of uncertainty. The number of pixels considered at each location varied from 26 to 5974 and an average of 710, according to the textural context. Larger crystal cores allowed for more pixels to be considered. Each QEMSCAN composition range is shown to be equivalent to ~2 Fo units (see Electronic Appendix 1).

Clinopyroxene trace element concentrations were measured from seven samples by laser ablation inductively coupled plasma mass spectrometry (LA-ICP-MS) at the Camborne School of Mines, University of Exeter, using a New Wave Research 213 nm Nd-YAG laser coupled to an Agilent 7700 ICP-MS. The laser was operated using a 50 μm spot, 40s dwell time and a repetition rate of 10 Hz, and a fluence of 3–4 J cm^{-2}. Data reduction was carried out using Iolite version 2.5 (Paton et al., 2011). Median ^{29}Si concentrations for pyroxene cores and rims, as obtained by EPMA, were used as the internal standard composition and NIST SRM 610 was used for calibration. Repeat analyses of reference materials BCR-2G and GSD-2G demonstrate the concentrations of almost all analysed elements fall within 10% of published values (see Electronic Appendix 2.). Clinopyroxene targets were selected at random from the analyses of macrocrysts already characterised by EPMA.

We performed thermobarometric calculations on clinopyroxene and amphibole compositions using EPMA data collected as part of this study as well as whole-rock and glass data from the 2021 Tajogaite eruption (Day et al., 2022; Scarrow et al., 2024; Longpré et al., 2025) and the 1971 Teneguía eruption (Klügel et al., 2005; Praegel & Holm, 2006; Barker et al., 2015; Weis et al., 2015). Clinopyroxene-liquid geothermobarometry was performed using the barometer of Neave & Putirka (2017) iterated with the thermometer presented in Equation 33 of Putirka (2008). These models are associated with prediction uncertainties (expressed as standard errors of estimate (SEEs)) of 140 MPa and 27 °C, respectively when tested against their calibration datasets. Although the barometer of Neave & Putirka (2017) was originally calibrated for use in tholeiitic systems, comparing our clinopyroxene and liquid (i.e., glass and whole-rock) compositions with the compositions used for model calibration demonstrate that it can be useful in moderately alkalic systems like the 2021 Tajogaite eruption (Electronic Appendix 2).

Iterative clinopyroxene-liquid matching was performed using the thermobar python package (Wieser et al., 2022). Clinopyroxene compositions were matched to tephra glass compositions from the 2021 Tajogaite eruption on the basis that these represent true, if compositionally variable, magmatic liquids erupted from the plumbing system. Calculations were performed with three different barometer-thermometer pairs to check for internal consistency: the barometer of Neave & Putirka (2017) paired with the thermometer presented in Equation 33 of Putirka (2008), the barometer presented in Equation 31 of Putirka (2008) paired with the thermometer presented in Equation 33 of Putirka (2008) and the P1 barometer of Putirka et al. (1996) paired with the T1 thermometer of Putirka et al. (1996). Ultimately we found that all three barometer-thermometer pairs returned equivalent results within uncertainty, and so present the results of calculations performed with the barometer of Neave & Putirka (2017) in the main text (results from all model pairs are provided in Electronic Appendix 2).

Equilibrium clinopyroxene-liquid pairs were estimated in two ways that both assumed that all Fe was present as Fe^{2+} (e.g., Wieser et al., 2023). Firstly, matches were identified following the a slightly modified approach of Neave et al. (2019): pairs were considered to be in equilibrium when they were within 1SEE of DiHd and EnFs equilibrium (±0.06 and ±0.05, respectively) according to the models of Mollo et al. (2013), 1SEE of CaTs equilibrium (±0.03) according to the model of Putirka (1999) and 1SEE of $Kd^{(Fe\text{-}Mg)}$ equilibrium (±0.08) according to Equation 35 of Putirka (2008). Following this approach we found that analyses from low-Al hourglass sectors in clinopyroxene rims returned pressures ~500 MPa lower than analyses of high-Al prism sectors in the same rims. As such, Na partitioning between hourglass and prism sectors in clinopyroxene crystals from Tajogaite fundamentally affects thermobarometric calculations. Interestingly, offsets between sectors have been noted in some alkaline systems (e.g. Haleakala, Hammer et al. 2016), but not others (e.g. Etna, Ubide et al., 2019). As such we exclude analyses from sectors containing <6.5 wt.% Al_2O_3 from subsequent discussions as they likely represent compositions formed during disequilibrium crystallisation (Neave et al., 2019). Secondly, and to avoid imposing bias by excluding data based on a simple compositional filter, we identified matches following the approach of Macdonald et al. (2023): pairs were considered to be in equilibrium when they were within approximately 2SEE of DiHd equilibrium and 1SEE of EnFs equilibrium (±0.10 and ±0.05, respectively) according to the models of Mollo et al. (2013), and 1SEE of CaTs and CaTi equilibrium according to the models of Putirka (1999). Importantly, this approach appears to rigorously reject analyses from low-Al hourglass sectors, and returns, to first order, magma storage conditions within uncertainty (1SEE; ±140 MPa and ±27 °C) of those estimated with the approach of Neave et al. (2019).

Additional amphibole-only thermobarometry was performed using the barometer of Ridolfi (2021) and the thermometer of Ridolfi & Renzulli (2012). The quoted uncertainties for these methods are12% relative and 22 °C, respectively, although tests on independent calibration datasets reveal larger errors (Wieser et al. 2025). However, unlike clinopyroxene crystals that are found in products from throughout the eruption, analysable amphibole crystals were only found in products from the earliest days of the eruption, and thus provide a partial record of magmatic processes.

To undertake diffusion modelling, orientations of olivine mineral grains were determined by electron backscatter diffraction (EBSD) methods using a FEI Quanta 650 Field Emission Gun-

Environmental Scanning Electron Microscope (FEGSEM) at the University of Leeds, and the Zeiss Gemini 450 FEGSEM in the SEM Shared Research Facility at the University of Liverpool. Backscattered electron (BSE) images of zoned olivine grains were collected at the University of Derby (on a Tescan Vega 3 SEM) and the University of Liverpool (on a Zeiss Gemini 450 FEGSEM). Greyscale profiles of Fe-Mg in olivine were extracted from BSE images using ImageJ® software. The greyscale values were then tied to Mg# [Mg# = 100 × Mg / (Mg + Fe)] using analysed EPMA spots, and then modelled using Autodiff following the method of Couperthwaite et al., (2020). 17 crystals from a single tephra sample were used for diffusion modelling, at two temperatures of 1125 °C and 1150 °C, representing the systemic range in modelled clinopyroxene-melt thermometry, 860 MPa pressure, from clinopyroxene-melt barometry (above), and fO_2 at NNO+1 within the range of oxygen fugacities published on the Tajogaite eruptions (Frascerra et al., 2024) and from the previous two eruptions from La Palma with intensive variables from past eruptions (Klügel, 1998; Klügel et al., 2000; Barker et al., 2015). The range of past oxygen fugacities varies by ~ 3.0 log units, we have used a single value for a single sample; more oxidising conditions would result in shorter modelled timescales, more reducing conditions would result in longer modelled timescales. Each Mg# profile was extracted perpendicular to the imaged crystal edge, and the orientation of this profile relative to crystallographic axes (established from output Euler poles in EBSD analyses using the spreadsheet Eulerproc, available on request from DJM) was input into the AUTODIFF model to account for the known anisotropy of Fe-Mg interdiffusion in olivine (Couperthwaite et al., 2020). Uncertainties on modelled timescales were calculated using a Monte Carlo simulation incorporating a ±30 °C analytical uncertainty on temperatures, and associated uncertainties on true pixel size, the number of integrated pixel lines across each boundary, fO_2 uncertainty (± 0.3 log units), and the greyscale intensity used to define the Mg# values.

Results

Whole-rock framework

It is clear from published data that magmas erupted during the Tajogaite eruption are exclusively silica-undersaturated mafic alkali basalts in composition (Pankhurst et al., 2022, Day et al., 2022, Ubide et al., 2023, Scarrow et al., 2024). Within this restricted compositional range and as a result of detailed time-series sampling, Scarrow et al. (2024) identified three key stages within the eruption progression based on temporal trends in whole-rock element concentrations and ratios. The identification of three stages is supported by other published data including radiogenic isotope work, geophysical data, and fluid inclusion data (Fig. 2, Day et al., 2023; Dayton et al. 2023, Ubide et al., 2023; Zanon et al., 2024; Scarrow et al., 2024), and can be summarised as follows (Fig. 2):

- Stage 1- Eruption onset to ~Day 5: This stage is marked by significant changes in erupted magma compositions over a short duration, with whole-rock MgO increasing between 6.0 and 6.7 wt/%, coupled with increases in Ni from 50 to 65 ppm, and decreasing Zr (355 - 340 ppm; Scarrow et al., 2024). At this time, groundmass materials have highly radiogenic $^{87}Sr/^{86}Sr$ (Ubide et al., 2023) and radiogenic $^{187}Os/^{188}Os$ (Day et al., 2022).
- Stage 2- ~Day 7 to ~Day 67: During this stage whole-rock MgO and Ni concentrations rise from 7.5 to 8.6 wt.% and from 85 to 130 ppm respectively (Scarrow et al., 2024). This rise continues to ~ day 18 when MgO (and coupled elements) plateaus, and the erupted magma compositions stabilise. The general increase and stabilisation in MgO is matched by Sr isotopic data, with a systematic trend from $^{87}Sr/^{86}Sr$ of ~0.70315 to ~0.70307 in the first ~half of the eruption. Ratios from the last ~half of the eruption are reported as forming two parallel trends at ~0.70312 and ~0.70304 (Ubide et al., 2023). $^{187}Os/^{188}Os$ similarly stabilise at less radiogenic ratios (Day et al., 2022).
- Stage 3- ~Day 70 to eruption end: this stage is only evident in whole-rock and glass (and matrix) compositions, and is marked by an inflection and then decrease in MgO concentrations from 8.6 to 8.0 wt.% (alongside Ni, TiO_2, and increases in K_2O, Al_2O_3, Na_2O, Zr, Ba, Sr; Scarrow et al., 2024). No change is evident in the existing radiogenic isotope data (Day et al., 2022, Ubide et al., 2023), which may be due to limited sample coverage for those data during this time period.

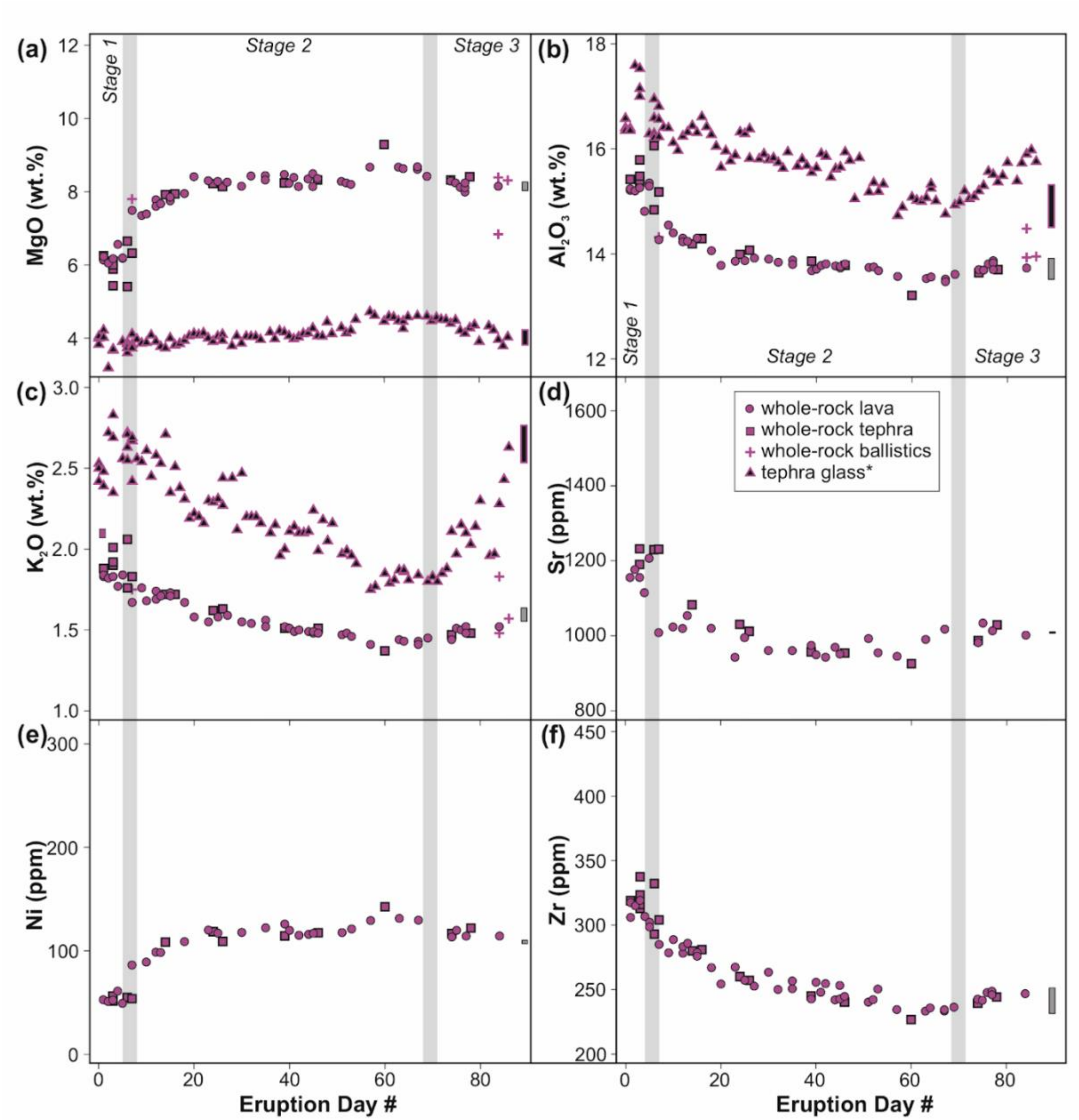

Figure 2: Published whole-rock major and trace element data from Scarrow et al (2024) and tephra glass data (*) from Longpré et al., (2025). Three identified stages from Scarrow et al. shown as grey vertical bars. Uncertainties on analyses are shown as the grey bars on the right side of graphs (Scarrow et al., 2024) or as black bars (Longpré et al., 2025).

QEMSCAN

Products erupted in the first few days (i.e. Stage 1) host a polymineralic crystal cargo of clinopyroxene, amphibole, titanomagnetite, minor plagioclase, and rare olivine (Pankhurst et al. 2022). Crystals occur as polyhedral clusters up to 3 mm in length as well as individual crystals up to 2 mm in most samples, with most (and all titanomagnetite and olivine) being < 0.5 mm (Table 2, Fig. 3). Products from Stages 2 and 3 are characterised by comparatively invariant abundances and textures of clinopyroxene and olivine up to a few mm in length, where the amount of plagioclase is sensitive to the degree of late-stage cooling experienced before quenching, discussed below. All samples exhibit a seriate texture (see Electronic Appendix 1 for plots of crystal size distribution through time), and we find that 10,000 μm^2 is a useful distinction between macrocrysts and microcrysts to represent the variations in crystal sizes observed across all mineral phases. All percentages reflect areal % of examined thin sections. Figure 4a illustrates that macrocrystic olivine abundance increases from zero to 5% over the first ~10 days and then is stable at 5% (with maxima of 6.8 and minima of 3.6) for the remaining eruption duration. Likewise, clinopyroxene increases from 6.3% to 11.5% in the first ~10 days, and is also comparatively stable at 12.5% for the duration (varying between 17% and 9.7%).

Amphibole is reported by the QEMSCAN® protocol throughout the eruption in the groundmass and as visually identified macrocrysts in the earliest of samples and the very last (one fully recrystallised instance in sample CAN_LLP_0096, from day 79: Fig.3). The majority of pixels classified as amphibole are single and isolated, which is below the spatial confidence threshold. These data points likely represent fine-grained clusters of other phases (i.e. clinopyroxene, plagioclase, ilmenite, glass) below the pixel resolution whose individual signals are convolved to approximate an amphibole composition (evident in some samples where BSE images were collected). Amphibole pixels in obvious clusters well above the spatial confidence threshold typically exhibit rounded margins and variably patchy interiors. They are most abundant in CAN_LLP_0003 (day 3 of the eruption) but do not exceed >0.5% by area when connectivity is based on 4 neighbours or >0.7% when based on 8 neighbours. These clusters are interpreted as kaersutite (Pankhurst et al., 2022) that preliminary results suggest has been variably recrystallized to a combination of rhönite, plagioclase, clinopyroxene, and ilmenite. These results are the topic of further work that will not be discussed in greater detail here. In this contribution we show that these variably recrystallized amphibole clusters are only characteristic of the first few days of the eruption. We therefore consider macrocrystic amphibole (and/or its recrystallized products) to be a minor phase whose presence is a robust characteristic of Stage 1, and whose abundance decreases together with other petrological signals from Stage 1 to Stage 2. Titanomagnetite macrocrysts, like amphibole, are most abundant in Stage 1 (maximum 0.85%), and after a sharp decrease into Stage 2 (0.3%) steadily decrease throughout the eruption (Fig. 4).

Plagioclase is a ubiquitous phase and present in abundances from 4 to 25%, yet is exceedingly rare as macrocrysts and its abundance is controlled almost completely by the degree of late-stage crystallisation. Its abundance comprises an average of 34% of the total microcryst percentage (min. 18%, max. 44%). When expressed as a percentage of the total microcryst abundance, plagioclase is confirmed as a very late crystallising phase, since those samples with the lowest amount of microcrysts (i.e. glassier groundmass) have disproportionately low plagioclase abundance (see Electronic Appendix 1). Plagioclase macrocrysts are calculated as exceeding 1% of rock area in several samples (Fig. 4), although this occurs only in samples where the total plagioclase is $>20\%$, and many instances may be artefacts of lath clustering that eluded watershed segmentation rather than reflecting true individual macrocrysts. We struck a balance between the complexity of the segmentation protocol and its final accuracy, and found that using a simple watershed avoided the misattribution of plagioclase clusters to macrocrysts even in the most plagioclase-rich groundmasses.

Olivine trends from rare fayalitic ($Fo < 77.6$) and microcrystic (0.17% macrocrysts of rock area) to forsteritic and macrocrystic ($Fo > 83.2$, 4.57% by day 12) from Stage 1 into Stage 2, and then maintains a comparatively consistent abundance and texture until the end of eruption (see Fig. 4 and Electronic Appendix 1).

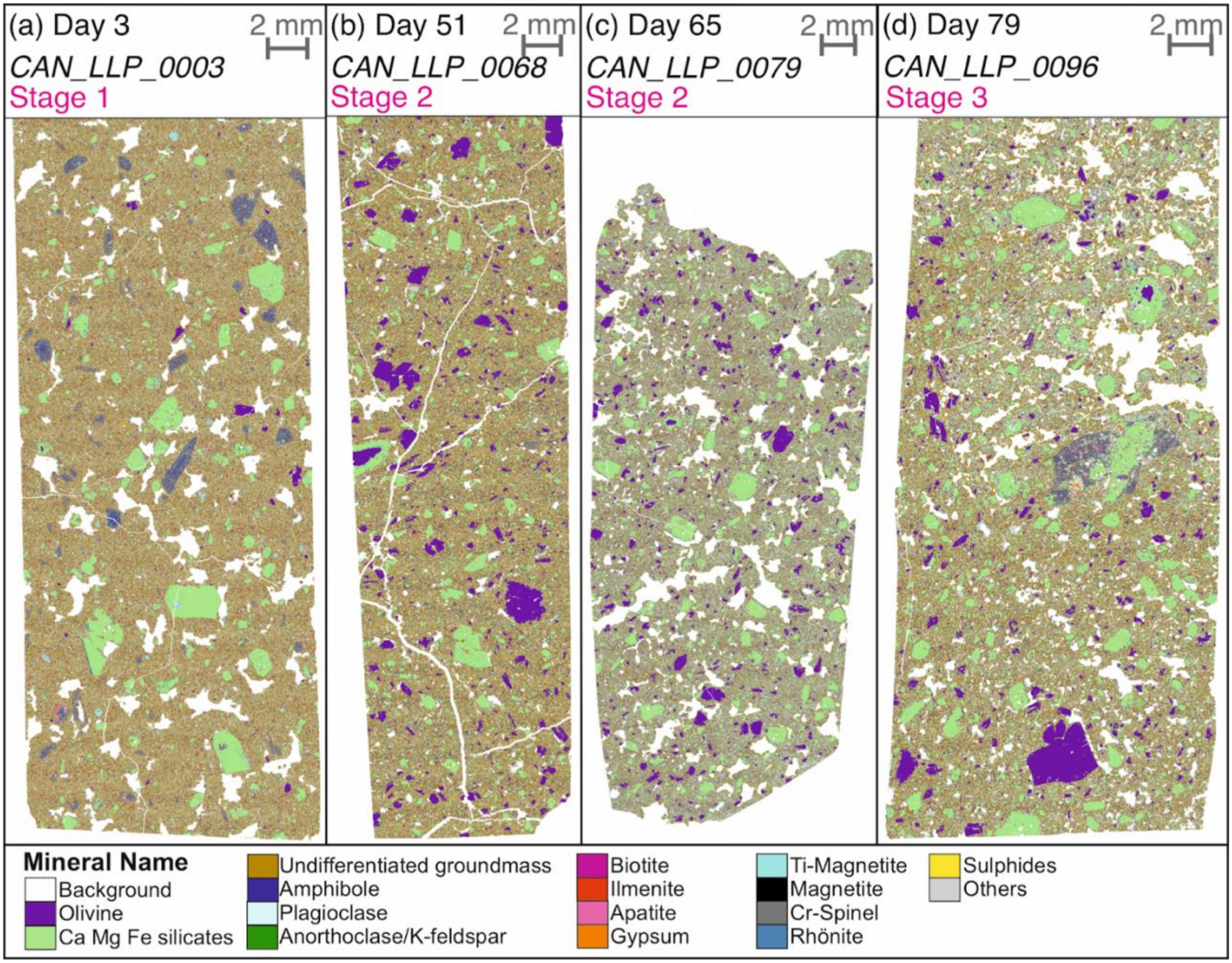

Figure 3: QEMSCAN® maps from Stage 1 (a), Stage 2 (b, c) and Stage 3 (d) lavas of the Tajogaite eruption. Clinopyroxene (light green) is the major macrocryst phase in all stages. Olivine becomes a major macrocryst phase from Stage 2. Amphibole occurs mainly as isolated macrocrysts in Stage 1 only, and is present only once again as part of one polymineralic cluster at the end of the eruption. Differences in groundmass texture (e.g. b: glassy vs c: microcrystaline) indicate the role that phase connectedness plays when calculating macrocryst percentages and underscores the importance of image segmentation. Inferred phases (see key) are a result of chemical identification using index-matching to the most likely minerals based on sample type, and confirmed by EPMA.

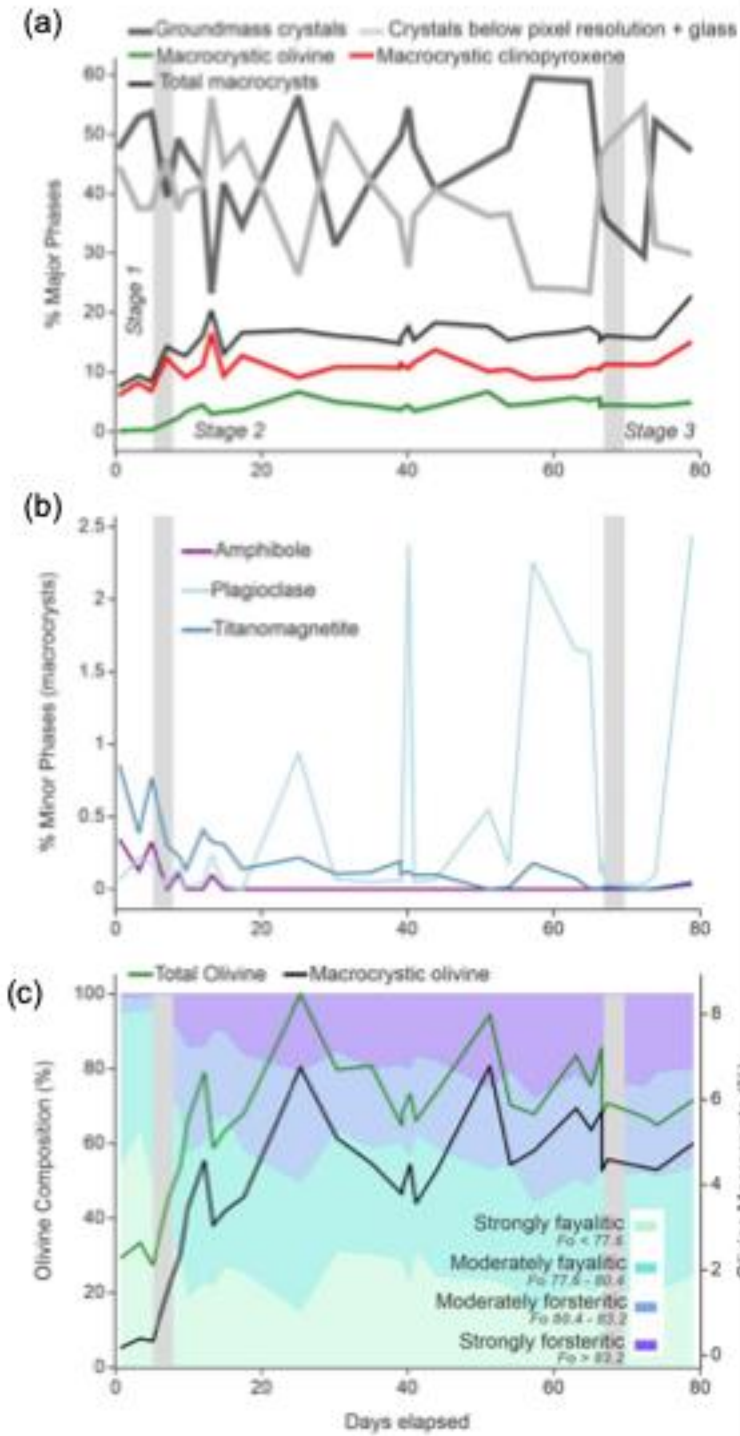

Figure 4: Temporal trends in mineral proportions and compositions during the Tajogaite eruption, as derived from QEMSCAN® analysis of lava samples, with key stages identified from Scarrow et al. (2024) shown as vertical grey bars. (a) Major mineral phases shown as macrocryst proportions (red, green and black, where macrocrysts refer to grains >10,000 μm²); (b) Selected minor macrocryst phase abundance (for full phase variation see Table 2); (c) Olivine compositional change over the eruption shown as proportions (coloured zones), compared with both total olivine and macrocrystic olivine abundance (green and black lines, secondary y-axis).

Mineral compositions

The compositional variation of macrocryst phases through eruption time are similarly restricted to that of their abundances and matches the timing of textural changes. In both tephra and lava samples, Stage 1 olivine cores and rims have generally much more restricted compositions than during the rest of the eruption sequence, with Fo 77.1 - 82.2 and NiO 0.03 - 0.19 wt.%. After Stage 1, olivine exhibits greater compositional diversity within individual samples, with Fo 70.5 - 85.9 and NiO between 0.05 - 0.30 wt.% (Fig. 5a). Olivine cores either overlap with or are slightly more primitive than rim analyses in all samples (Fig. 5b). There is no distinguishable difference in olivine compositions between Stage 2 and Stage 3. The complete major and trace element mineral dataset is reported in Electronic Appendix 3.

Clinopyroxene is the most abundant mineral phase throughout the Tajogaite eruption (Fig. 4) and exhibits a considerable range in composition, yet no obvious differences in clinopyroxene core or rim major element compositions are evident through the eruption progression (Fig. 6). Macrocrystic (>250 µm) clinopyroxene cores have diverse compositions with Mg# between 56 and 83, and TiO_2 concentrations in the range 0.85 - 4.84 wt.%. Rim and groundmass compositions have similar compositions; Mg# ranges from 55 to 79 and TiO_2 between 1.75 and 6.71 wt.%. Similarly to the major element compositions, there are no clear trends in clinopyroxene trace element concentrations or ratios with eruption progression (Fig. 6b, d). Stage 1 clinopyroxene cores span similar ranges in trace element concentrations to Stage 3 clinopyroxene. Stage 2 clinopyroxenes have similar trace element ranges, however the amount of variation within a single specimen varies between samples, which may reflect limited numbers of crystals analysed per sample.

In samples containing unaltered amphibole crystals (LLP_0001 and LLP_0003, from day 1 and day 3 of the eruption respectively), major element analyses show limited differences in amphibole compositions. $Ti_{(23O,\ apfu)}$ ranges between 0.58 and 0.72, and Mg# ($Mg_{(23O,\ apfu)}/(Mg_{(23O,\ apfu)}+Fe_{(23O,\ apfu)})$) between 0.62 and 0.72. These concentrations place the amphibole in the kaersutite field (Fig. 7a) and agree with the QEMSCAN® results. Amphiboles from day 3 of the eruptive sequence appear to have slightly higher Mg#s than those from day 1, but other major element concentrations (Ca, Na, Al(IV, apfu), $Ti_{(23O,\ apfu)}$) show substantial overlap between the two days (Fig. 7).

Major and minor element concentrations of tephra glass were collected from 5 samples that span eruption days 3 - 80 (see Table 1 for sample details) and compared with existing glass average compositions from Longpré et al (2025). Individual glass analyses reported here overlap with the average tephra glass analyses from the entire eruption duration, with SiO_2 concentrations in the range 43.6 to 49.1 wt.%, Na_2O+K_2O 6.08 - 9.22 wt.% and MgO 3.4 - 5.9 wt.% (Fig. 8). Earliest erupted tephras are the most evolved, with the highest SiO_2, total alkalis, and lowest MgO, FeO, and CaO/Al_2O_3. Tephra samples from day 60 are the least evolved of the sample analysed here, with tephra from day 80+ recording a slight increase in SiO_2 from day 60 (Fig. 8) - following whole-rock trends, where this change in SiO_2 is accompanied by a ~50% relative increase in K_2O in whole-rock analyses (Fig. 2).

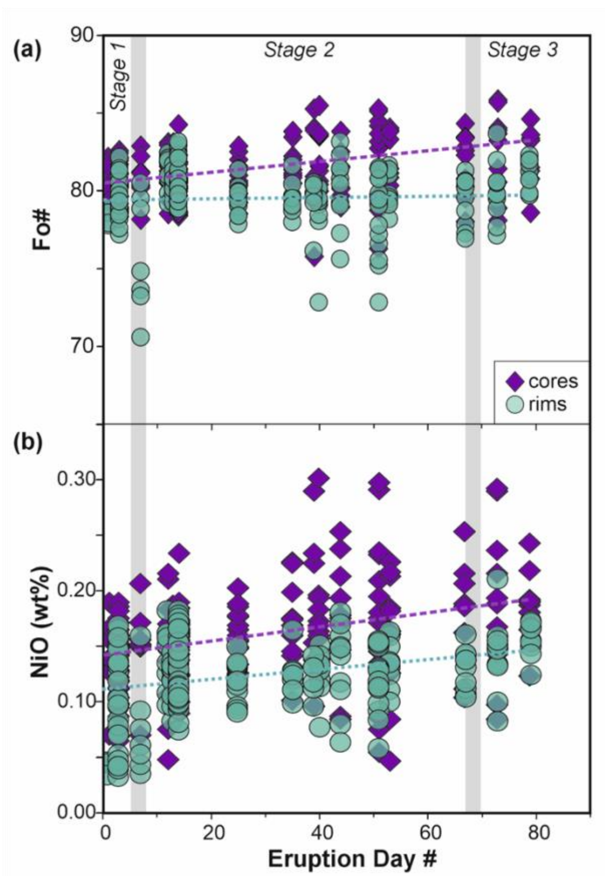

Figure 5: Olivine major element concentrations by core (purple diamonds) and rims (turquoise circles) presented according to eruption time, measured by EPMA. Dashed lines are linear regressions. Stages identified from whole-rock geochemistry (Scarrow et al., 2024) shown as vertical grey bars. Calculated uncertainties in NiO and Fo are always less than the size of symbols. For full details of precision and accuracy see Electronic Appendix 2.

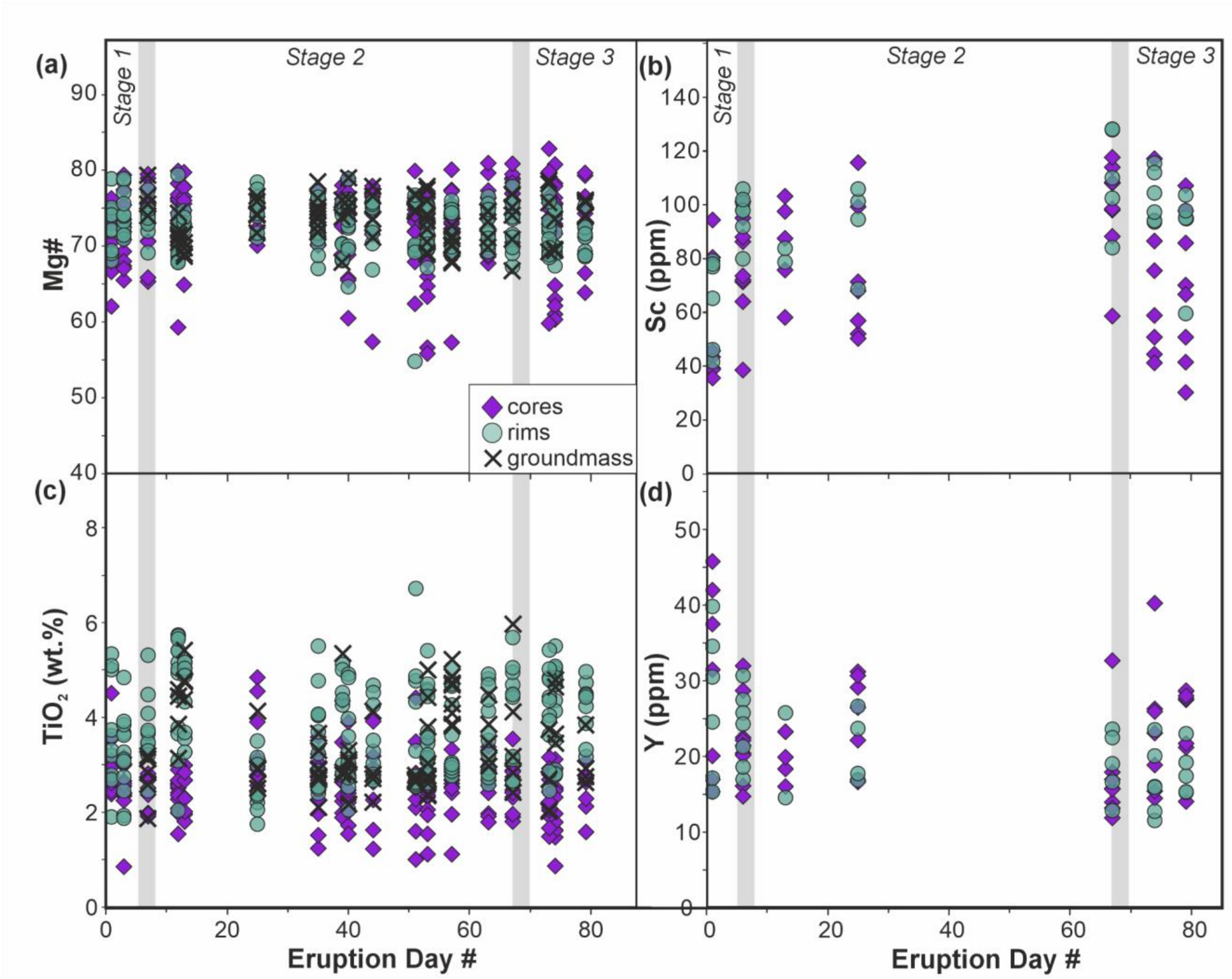

Figure 6: Clinopyroxene major (a, c, by EPMA) and trace element (b, d by LA-ICPMS) concentrations grouped by core (purple diamonds), rims (turquoise circles) and groundmass (black crosses) over time. Stages identified from whole-rock geochemistry (Scarrow et al., 2024) shown as vertical grey bars. Calculated 2σ uncertainties in Mg#, TiO_2, Y and Sc are always less than the size of symbols. For full details of precision and accuracy of data see Electronic Appendix 2.

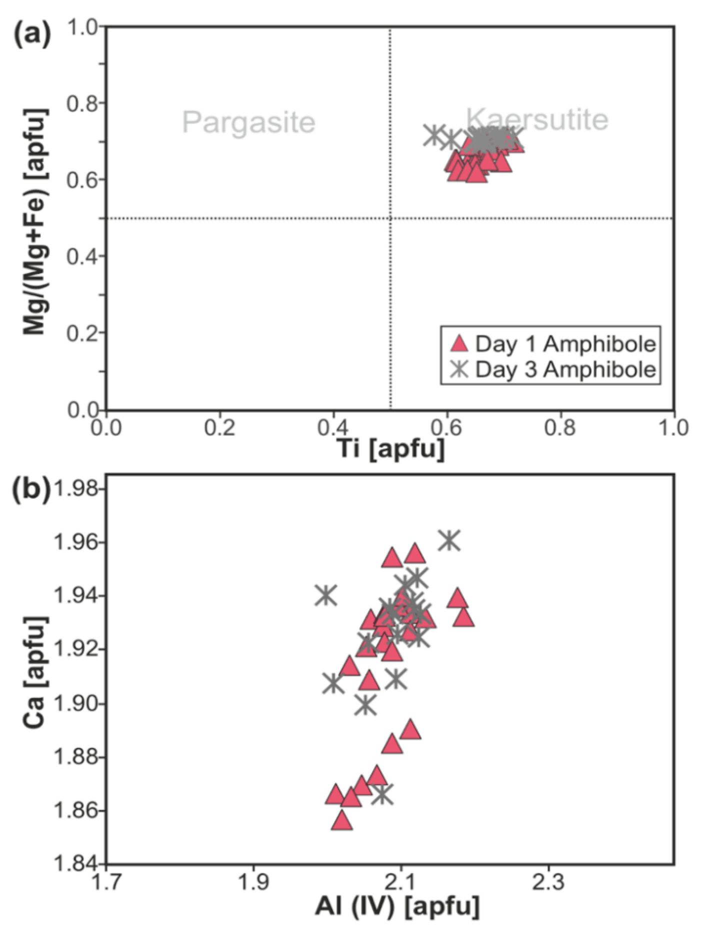

Figure 7: Amphibole major element concentrations measured by EPMA grouped by eruption day: day 1 pink triangles, day 3 grey crosses. Classification follows Leake et al., 1997.

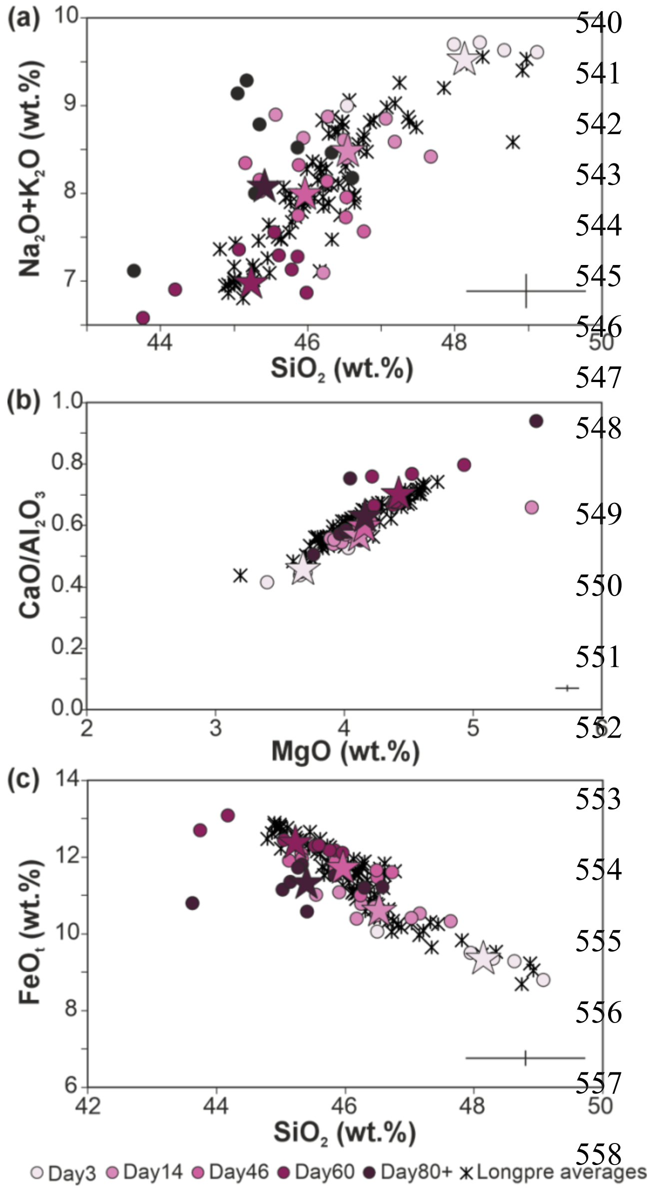

Figure 8: Tephra glass major element concentrations measured by EPMA. Analyses are grouped by eruption day, with lighter colours relating to earlier samples. Individual glass analyses (circles) and their average values (stars) are compared with averages of tephra glass samples (black crosses, Longpré et al., 2025) throughout the eruption. Black error bars represent uncertainty from standard analyses (see Electronic Appendix 2 for details).

Thermobarometry

Considering model uncertainty, results of clinopyroxene-liquid geothermobarometry suggest that clinopyroxenes were sourced from magmatic environment(s) in the upper mantle (Fig. 9). Pressure and temperature calculations of clinopyroxene rims and groundmass crystals return mean values of 860 ± 70 (1σ) MPa and 1128 ±11 8 (1σ) °C, and 786 ±91 (1σ) MPa and 1123 ±8 (1σ) °C, respectively, following the equilibrium matching approach of Neave et al. (2019), and mean values of 768 ±72 (1σ) MPa and

1121 ± 6 (1σ) °C, and 727 ±51 (1σ) MPa and 1115 ±8 (1σ) °C, respectively, following the equilibrium matching approach of Macdonald et al. (2023). Regardless of the equilibrium matching approach used, mean pressures and temperatures from these textural populations are within uncertainty of each other once prediction uncertainties associated with model calibrations are considered (1 SEE prediction uncertainties associated with the barometer and thermometer are quoted at 140 MPa and 27 °C, respectively, although the uncertainty could be larger cf. Wieser et al., 2023). The range of pressures recorded by clinopyroxene rims also do not change through the course of the eruption. These qualitative observations indicate a continuity of process despite the likely quantitative inaccuracy.

Clinopyroxene cores are chemically and texturally distinct from the rims, being richer in Na at any given Mg#, extend to lower Mg#, and also exhibit less clear evidence of sector zoning (Fig. 9a). Where clinopyroxene cores are in chemical equilibrium with glass analyses, they record mean pressures and temperatures of 833 ± 68 (1σ) MPa and 1127 ± 6 (1σ) °C, and 833 ± 53 (1σ) MPa and 1126 ± 8 (1σ) °C, respectively, following the approaches of Neave et al. (2019) and Macdonald et al. (2023), respectively (Figure 9). Sector zoning plays a clear role in thermobarometric assessments at La Palma- sectors with Al_2O_3 < 6.5 wt.% (typically {111}) return systematically lower pressures than clinopyroxene analyses with >6.5 wt.% Al_2O_3 (typical of {hk0}, Fig. 9a)

All of the clinopyroxene composition for which we could robustly identify equilibrium liquids returned pressures with a few 10s MPa of ~800 MPa, which corresponds to a depth of ~27 km. Importantly this overlaps with the upper limit of the deeper cluster of depths estimated from melt inclusion and fluid inclusion barometry (Fig. 9f; Dayton et al., 2023, 2024). That is, both clinopyroxene and volatile saturation approaches to barometry at Tajogaite return pressures that are comfortably within uncertainty of each other and confirm the importance of upper mantle magma storage in supplying the eruption.

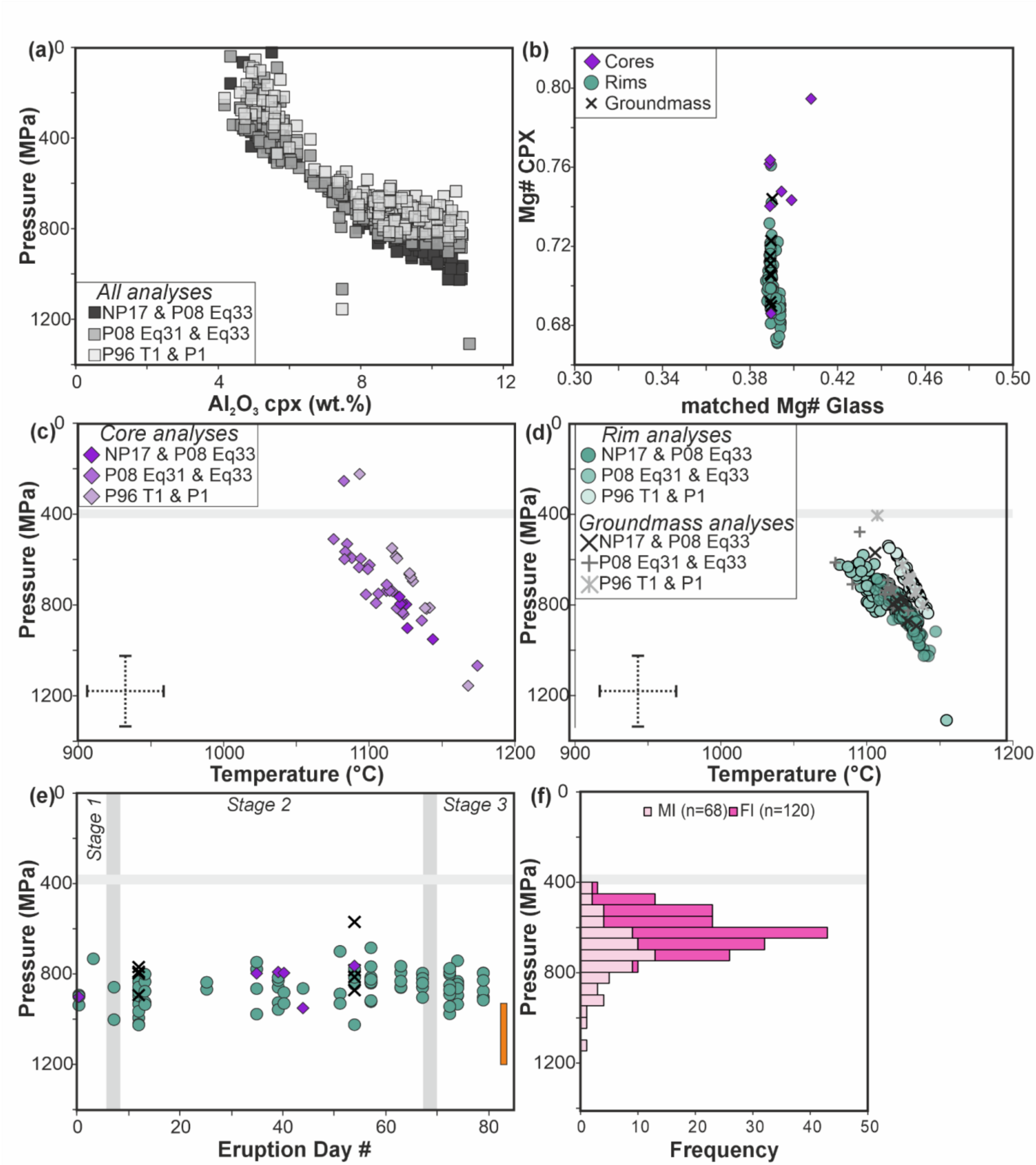

(a)
Pressure (MPa)
All analyses
NP17 & P08 Eq33
P08 Eq31 & Eq33
P96 T1 & P1
Al_2O_3 cpx (wt.%)
(b)
Cores
Rims
Groundmass
Mg# CPX
matched Mg# Glass
(c)
Core analyses
NP17 & P08 Eq33
P08 Eq31 & Eq33
P96 T1 & P1
Temperature (°C)
(d)
Rim analyses
NP17 & P08 Eq33
P08 Eq31 & Eq33
P96 T1 & P1
Groundmass analyses
NP17 & P08 Eq33
P08 Eq31 & Eq33
P96 T1 & P1
(e)
Stage 1
Stage 2
Stage 3
Eruption Day #
(f)
MI (n=68)
FI (n=120)
Frequency

587

Figure 9: Calculated crystallisation temperatures and pressures for clinopyroxene samples compared with clinopyroxene compositions (a, highlighting role of sector zoning) and then separated by cores (purple diamonds), rims (green circles) and groundmass (black and grey crosses) from selected samples (Table 1) throughout the eruptive sequence of 2021 Tajogiate eruption, with La Palma pressures for the Moho shown as horizontal light grey bars (after Klügel et al., 2022). Three different calibrations were run (a, c, d) on cores, rims and groundmass analyses: Putirka et al., 1996 (P96 T1 & P1), Putirka 2008 (P08, Eq 31 & Eq 33) and Neave and Putirka, 2017 for pressures, and Putirka 2008 for temperatures (NP17 & P08 Eq 33). Only the results from application of Neave & Putirka (2017) combined with Putirka (2008) are shown in (b, e). Stages identified from whole-rock geochemistry (Scarrow et al., 2024) shown as vertical grey bars in (e). Uncertainty on modelled values from propagating analytical uncertainty are shown as dashed crosses (c,d) or an orange bar (e) following Wieser et al. (2023). Melt inclusion (MI) and fluid inclusion (FI) barometry shown in (f) from Dayton et al. (2023, 2024).

Amphibole crystals from the earliest phases of the eruption return mean pressures and temperatures of 535 ± 20 (1σ) MPa and 1043 ± 7 (1σ) °C. While these values are lower than those estimated from clinopyroxene crystals, pressure values are within 2SEE of values of those estimated clinopyroxene crystals (2SEE uncertainties of amphibole and clinopyroxene barometers are 120 MPa and 280 MPa, respectively). In contrast, amphibole crystals probably do record meaningfully lower temperatures than clinopyroxene textures (2SEE uncertainties of both the amphibole and clinopyroxene thermometers are 27 °C). Indeed, the textural relationships between amphibole and surrounding minerals (see above section 4.2) suggest amphibole and clinopyroxene could be from different environments, reinforcing the differences in estimated pressures and temperatures.

Olivine zonation and diffusion chronometry

Textural diversity is observed within olivine macrocrysts despite the variation in core and rim compositions overlapping within individual samples (Figure 5). The abundance of normal, reverse, and unzoned olivine crystals varies throughout the eruption sequence. Systematic changes in olivine textures are observed in tephra samples, and are comparable with the changes observed in the olivine textures in lava samples characterised by QEMSCAN (Fig. 4). Stage 1 olivine in tephra is characterised by thin normal zonation (Fig. 10a, b) with evidence for dissolution in the form of curvilinear crystal edges and widening re-entrants (Fig. 10b) in 65% of the olivine crystals images in day 3 tephra samples. In Stage 2, reverse zoned olivines become apparent, comprising up to 50% of imaged olivine grains in early Stage 2. This proportion then appears to decrease through Stage 2 and into Stage 3 with unzoned grains dominating by day 74 (Fig. 10a, d). By the end of the eruption, the latest in-situ tephra have only normal zoned and unzoned olivines, again with >15% of the studied crystals showing evidence of dissolution (n=48, Fig 10a).

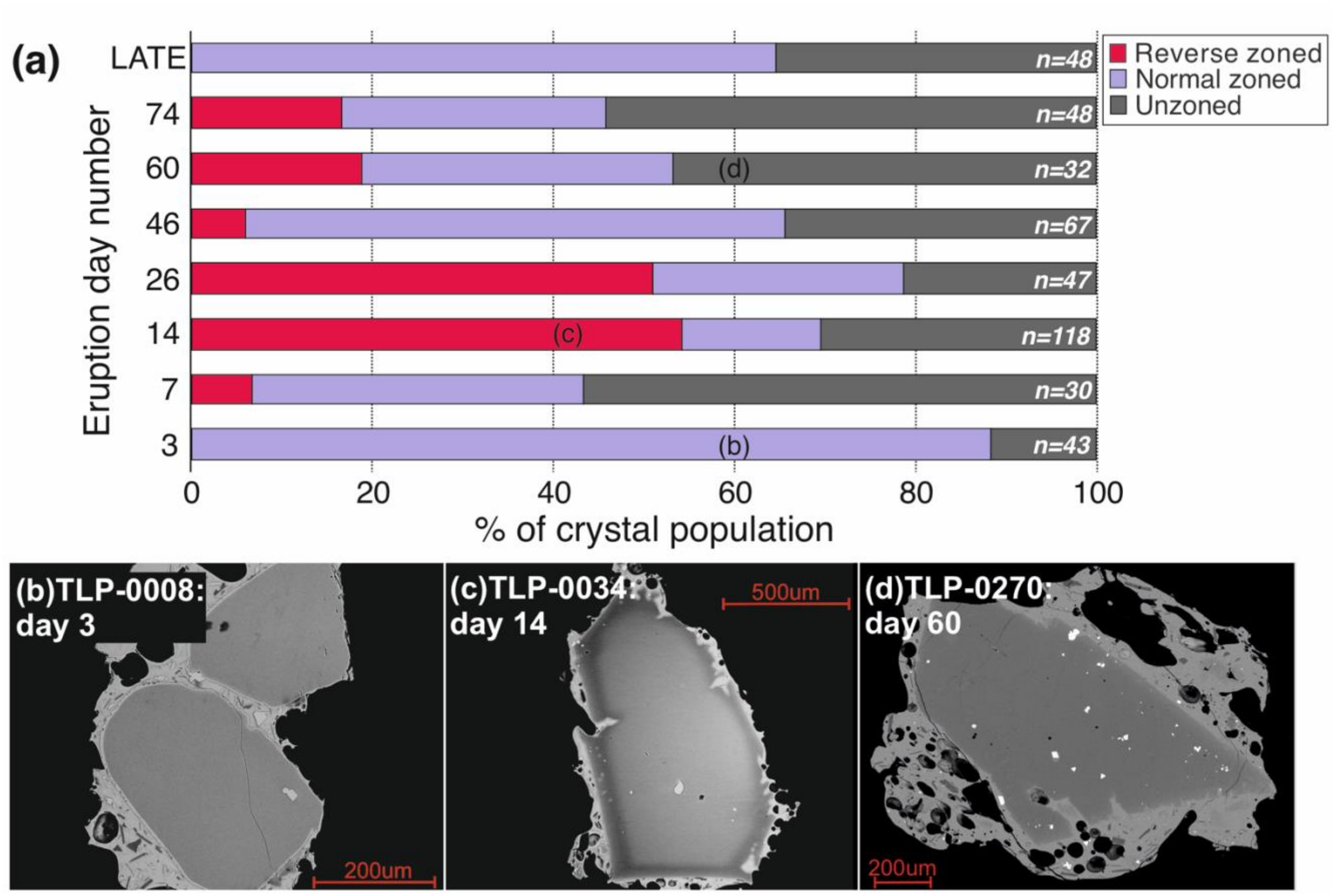

Figure 10: Textural variation of olivine macrocrysts in tephra samples throughout the Tajogaite eruption. (a) shows the proportions of olivine that are reverse-zoned (red), normally-zoned (purple) or unzoned (grey) against the day of the eruption (from 0-85). Number of crystals characterised per sample shown in white italics at the end of each bar. Representative examples of normal (b), reverse-zoned (c) and unzoned (d) macrocrysts are shown in BSE imagery with individual scales on each image. (b) and (d) also display late-stage dissolution textures.

In samples showing olivine zonation, preliminary modelling of timescales for diffusional relaxation was undertaken following the procedures of Chamberlain et al., (2024, see methods for details of intensive variables used). Only tephra olivines are considered here to minimise the effect of any post-eruptive mineral growth and diffusive relaxation in olivines erupted in lava flows (cf. Couperthwaite et al., 2021). Reverse zoning was modelled from sample TLP-0034 (eruption day 14) on 17 crystals yielding timescales <120 days, with 16 crystals yielding timescales <60 days, at temperatures of 1125°C (or timescales <80 days, with 16 crystals yielding timescales <40 days, at 1150°C). If the 14 days since eruption onset is removed, this suggests that these minerals record changes in the magmatic plumbing system occurring in the final few days to weeks prior to eruption (Fig.11). Only core to reverse zone profiles were modelled, as outermost Fe-rich zones cannot be explained by simple 1D diffusion models, and are likely a product of decompression-mediated overgrowth during ascent and eruption- which may add a few hours to days to modelled timescales (Romero et al., 2022, Bonechi et al., 2024). Further work to include the normal-zoned rim, and to determine how consistent the origin of reverse zone timescales are throughout the eruption is necessary to investigate crystal transfer mechanisms (cf. Pankhurst et al., 2018).

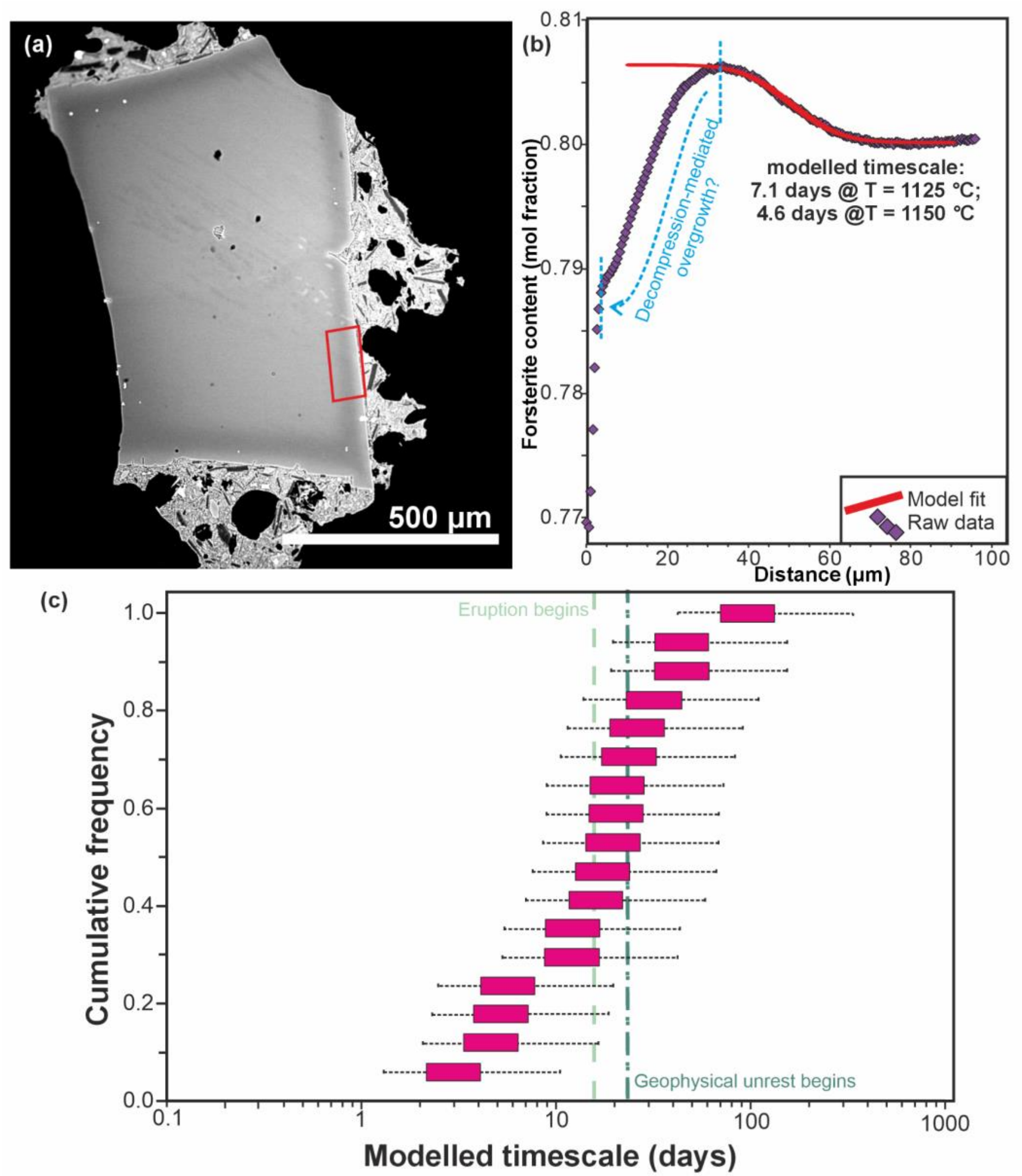

Figure 11: (a) Example of the reverse zoning preserved in olivine macrocrysts, with the area extracted for diffusion (red box) labelled; (b) corresponding Fe-Mg profile for the zone highlighted (purple diamonds), with the modelled fit to the raw data (red line); (c) compiled timescales of Fe-Mg interdiffusion modelling from reverse zones in sample TLP0034 (day 14 tephra). Pink bars represent the systematic uncertainty in timescales based on diffusion at 1125 and 1150°C. Dashed uncertainty bars represent combined uncertainty at 1 s.d. (see Methods for details).

Discussion

Extensive real-time geophysical, gas geochemical, and environmental monitoring data were collected during the 2021 Tajogaite eruption, but during the eruption no similarly time-resolved mineral-specific petrological data were available, inviting this retrospective study. Three stages have been identified from independent time-series of lava and tephra compositions and magma rheology studies, that coincide with initiation, progression, and waning (see section 4.1, Scarrow et al., 2024, Longpré et al., 2025, Day et al, 2022, Ubide et al., 2023, Soldati et al., 2024). The observation that compositional trends correspond to key eruption stages strongly supports the hypothesis that direct causative relationships exist between the architecture and evolution of magmatic plumbing systems and the behaviour of volcanic eruptions they generate, and, by extension, that these relationships are tractable through detailed petrological study. How these stages relate to the crystal record has not yet been examined systematically. Addressing this gap not only offers the potential to test published interpretations with the benefit of a more complete picture, from which more robust links to other subdisciplines could be made, but also has implications for considering what techniques to apply during future eruptions to generate forecasts of eruptive longevity, and when considering the approaches applied to pre-historic eruptions.

Generation and storage of Tajogaite magmas

Clinopyroxene is the most abundant, and ubiquitous, mineral phase in the 2021 Tajogaite eruption products (Fig. 4). The pressures and temperatures of crystallisation have been calculated by utilising clinopyroxene-melt thermobarometry (Putirka, 2008; Neave & Putirka, 2017). Clinopyroxene crystals return mean pressures on the order of 800 MPa (~27 km depth) in broad agreement with other barometry methods from both the 2021 eruption and past eruptions of La Palma (e.g. Ubide et al., 2023, see Scarrow et al., 2024 for full review of depth estimates), and are in line with geophysical estimates of magma storage at La Palma (D'Auria et al., 2022). Pressures from clinopyroxene cores overlap closely with values obtained from the 1971 eruption of La Palma (Klügel et al., 2005; Barker et al., 2015, of between 410 and 1410 MPa), and indicate that the upper mantle is an important site of magma storage and processing beneath La Palma, as it is beneath many other ocean island systems (Hansteen et al., 1998; Hildner et al., 2012; Kahl et al. 2021; van Gerve et al. 2024). Furthermore, clinopyroxene barometry indicates that magmas were sourced from the upper mantle throughout the eruption duration. That is, clinopyroxene rims record pressures that remain constant within uncertainty from the very first eruptive products to the last erupted material, suggesting that this deep storage zone plays a key role in driving all stages of the eruption. It is interesting to note that we cannot find evidence of shallower storage in the mineral record of the 2021 eruption, contrary to that found in geophysical studies (e.g. D'Auria et al., 2022) and melt and fluid inclusion work (Sandoval-Velasquez et al., 2023; Dayton et al., 2024; Zanon et al., 2024) where a zone of magma ponding at 6 – 16 km depth has been inferred.

It has been suggested that the initiation stage (Stage 1, 0 – 5 days) of the Tajogaite eruption was the result of a deeper magma invading a shallow alkali basalt (Scarrow et al., 2024), that had ponded and crystallised at ~6 – 16 km (Romero et al., 2022, Fabbrizio et al., 2023, Bonechi et al. 2024). Our analyses of early erupted products do not record these shallower pressures within clinopyroxene crystals, suggesting that whilst the amphiboles erupted in Stage 1 may have formed at shallow pressures, the clinopyroxenes that dominate the erupted crystal assemblage – with the possible exception of their outermost rims that were not captured by our analyses – were sourced from depth (Fig. 9). As such, the simplest explanation for our observations is that this magma crystallised clinopyroxene in an upper mantle reservoir before ascending to the shallow storage region where relict crystals could be accumulated.

Clinopyroxene core, rim and groundmass compositions are remarkably uniform throughout most of the eruption, even though cores are compositionally distinct from rims and groundmass crystals (Fig. 6). Moreover, we see no evidence for a slight deepening of magma storage zones tapped during the eruption (cf. Zanon et al., 2024 who suggest a deepening of the magma source region: from 600 - 750 MPa initially to 590 - 865 MPa as the eruption progresses) though minor shifts could be masked by the considerable uncertainties associated with clinopyroxene barometry. Indeed, reducing uncertainties and being able to robustly account for non-equilibrium crystal growth would translate to considerably greater interpretative power in our case. These areas for improvement notwithstanding, it is clear from the combination of the high temporal-resolution data presented here, and other published barometry, the deep source region at ~27 km depth persists throughout the eruption, which has important implications for reconstructing magma plumbing system models.

Eruption triggering and magma ascent

How long magma is stored in deeper crystallisation zones and what then triggers this magma to ascend and erupt are important questions whose answers may allow improved forecasting of future eruptive activity at La Palma and further afield. Using macrocryst textures and compositions alongside diffusion chronometry timescales yields insights into these processes. Interactions between resident and fresh influxes of magma are thought to have triggered eruptions in many types of systems (e.g., in the 1959 Kīlauea Iki episode: Sides et al., 2014; during the increased explosive phase of eruption from Turrialba 2014 - 2019: DeVitre et al., 2019, or the 2018 eruption from Kīlauea: Mourey et al., 2023; also see review in Perugini, 2021). Triggering can occur through increasing the overpressure of a system through volume addition, driving bubble nucleation, or fluxing of volatiles to increase the buoyancy of the melt (Cassidy et al., 2018, Caricchi et al., 2021) for which distinct populations of crystal chemistries in the same eruptive products provide compelling evidence. However, at Tajogaite, the earliest erupted macrocrysts do not have convincing evidence for magma mixing of this kind (i.e. as reverse zones in olivine). Some authors have noted reverse-zoned clinopyroxene in the earliest erupted material (Ubide et al., 2023), yet we observe no evidence for distinct populations of either cores or rims of clinopyroxene which could be attributed to distinct magma sources, and textural quantification of the zoning present is not presented by previous authors.

Instead, early destabilisation towards triggering and evidence for magma mixing are observed in later erupted material from Stage 2 (Fig. 2) onwards- although the process began before geophysical detection of unrest (Fig. 11). Reverse zonation became the dominant olivine zonation pattern in the first two tephra samples studied in Stage 2 (erupted on day 14 and day 26) - suggesting that later erupted material records the influx of more primitive magmas. This signature then wanes through the eruption, before disappearing in the last days of the eruption (CAN_TLP_0445, Fig. 10).

Diffusion chronometry focussing upon the timing of initiation of the reverse zones returns timescales on the order of a few days to tens of days prior to eruption onset, with only four of the 17 crystals recording diffusion that initiated after eruption onset (i.e. <14 days at 1125 °C, Fig. 11). These timescales overlap with, and extend, the period of climactic unrest detected immediately before the eruption (~7 days of increased seismicity and ground deformation; Carracedo et al., 2022; Civico et al., 2022; Romero et al., 2022; Wadsworth et al., 2022, Suarez et al., 2023). The overlap between diffusion timescales and timescales of climactic geophysical unrest suggest that both represent the final staging events that record the destabilisation of the magmatic system, which was ultimately triggered to erupt. As the diffusion timescales extend to earlier times than that of immediately pre-eruptive geophysical signals, the process of destabilisation began before its detection by geophysical methods.

Narrow normal (higher Fe) zones with or without evidence of dissolution are present at the very rim of many olivine crystals (Fig. 10). These zones cannot be modelled with simple 1-D diffusion models, and instead may reflect disequilibrium growth and diffusion on ascent (cf. Couperthwaite et al., 2021). Detailed combined modelling of these rims (alongside modelling of clinopyroxene zones) in future studies is required to place temporal constraints on this process (e.g. Couperthwaite et al., 2021, 2022; Bell et al., 2023; Kahl et al., 2023), but other studies of ascent during the Tajogaite eruption have suggested ascent of magmas from their storage in the mantle to the surface was of the order of 0.01 – 0.1 m/s, with more rapid ascent occurring in the upper crust (Romero et al., 2022; Bonechi et al., 2024; Zanon et al., 2024).

Extended periods of unrest were observed at La Palma for more that 4 years prior to the 2021 Tajogaite eruption; yet if these relate to magmatic injection and mixing between resident and intruding magmas, then they are not recorded in olivine macrocrysts, which typically lack internal zonation (Fig. 10). In contrast, clinopyroxene macrocrysts can exhibit complex zonation (including both oscillatory zoning, and sector zoning in rim domains). It is therefore likely that magmas (and crystal cargos) resided at high temperatures for long enough for evidence for past periods of magma interaction to be eradicated from olivine macrocrysts (cf., Thomson & Maclennan, 2013), but preserved in clinopyroxenes, in which the inter-diffusivity of Fe-Mg is approximately three orders of magnitude slower than in olivine at 1125°C (Dimanov & Sautter, 2000; Dohmen & Chakraborty, 2007; Couperthwaite et al., 2020).

Role of crystal cargo in modulating the 2021 Tajogaite eruption composition

Published studies of the 2021 Tajogaite eruption have identified three key stages from either whole-rock analyses (e.g. Scarrow et al., 2024), melt compositions (Longpré et al., 2025) or averaged matrix analyses (Ubide et al., 2023). By studying the role of the mineral record in defining these stages, we can deconvolve the glass, mineral, and whole-rock record. This will help to understand the processes behind the different eruptive stages, and facilitate developing a strategy for how to use mineralogical data in future eruption monitoring.

The mineral record clearly covaries with the change in eruption products from Stage 1 to Stage 2 (transition occurring over days 5-10) identified from other geochemical analyses (Fig. 2, 12; Day et al., 2022, Ubide et al., 2023, Scarrow et al., 2024). QEMSCAN data of the volumetrically dominant phases illustrate a pre-eruption magmatic plumbing system requiring no more than two crystal assemblage sources: an amphibole-bearing and olivine-poor (and fayalitic) assemblage; and an amphibole-absent and comparatively (forsteritic) olivine rich assemblage. The amphibole-bearing assemblage was erupted first, but soon after was either exhausted or bypassed by the forsteritic olivine-bearing assemblage, which continued to be erupted until cessation. The earliest erupted lavas and tephras contain a lower abundance of olivine crystals, which are more-evolved (Fig. 4), with no evidence for magma mixing in macrocryst phases (Figs. 10 & 11), and amphibole as an unstable phase (Fig. 7); yet, as discussed above, there is no observable change in the compositions or modelled pressures from clinopyroxene macrocrysts between Stage 1 and Stage 2. The more-evolved glass compositions (Fig. 8; Longpré et al., 2025) of tephras from Stage 1, alongside the presence of amphibole, and some comparatively low Fo olivine (Fig. 4), substantiate that the first erupted magma was subtly more evolved and more hydrous (Dayton et al., 2024). Stage 1 products possibly contain components of a residual magma from previous eruptions (Day et al., 2022; Romero et al., 2022; Fabbrizio et al., 2023; Ubide et al., 2023; Bonechi et al. 2024; Zanon et al., 2024; Scarrow et al., 2024). The presence of amphibole and low-forsterite olivine together with the potential for the addition of remelted crustal components or remobilised magma explains the more evolved nature of whole-rock composition and variability observed in tephra glass compositions in Stage 1 (Fig. 12).

Despite the difference in whole-rock compositions, we see no evidence for compositional changes in clinopyroxene macrocrysts in Stage 1 compared to Stage 2, which requires explanation. If the argument is made for a distinct, older, more evolved and more hydrous magma being erupted from shallower levels at the initiation of the eruption, we must explain why it contains the same clinopyroxene that is present in subsequent fresh and more primitive products from deeper in the system. One answer could be that the clinopyroxene that was erupted early was sourced from the same deep region. This would then imply that this clinopyroxene is residual from previous eruptive/intrusive events together with the rest of the Stage 1 magma because it did not crystalise in the shallow region it retains its deep signature. Why there is no clinopyroxene in Stage 1 that reflects the shallower storage level could be explained by equilibrium growth being suppressed in that environment with amphibole crystallisation at lower temperatures favoured instead. Suppression of clinopyroxene growth in a shallow system or in an ascending magma is consistent with the strong pressure dependence of clinopyroxene stability (e.g., Neave & Maclennan, 2020). The comparatively rapid ascent rates calculated for this eruption and slow diffusivity may have not allowed for clinopyroxene to record the interval between their growth at depth and further crystallisation at final cooling post-eruption, rendering them as largely inactive particles in shallow storage intervals and the active magma. By contrast, olivine and amphibole are faster to respond to the changes in the active magma's intensive parameters (i.e. Fe-Mg interdiffusion and breakdown respectively, see Didonna et al. (2024) and Devine et al. (1998)).

Contrary to the transition from Stage 1 to Stage 2 there is no striking transition from Stage 2 to Stage 3 in the macrocryst assemblage or in macrocryst abundances. There are also no compelling changes in measured mineral compositions, abundances or textures during Stage 3. The petrological signal between Stage 2 and 3 is defined by melt (Longpré et al., 2025) and whole-rock (Scarrow et al., 2024) compositions. The more evolved microcryst and rim compositions observed by Ubide et al. (2023) were suggested by those authors to indicate fractionation of the magma source, which they associated with eruption cessation but without a mechanism as to why. We suggest that these evolved microcrysts and rims as may have formed during late-stage ascent and lava emplacement, and so view their more evolved compositions as simply reflective of their more evolved carrier melts (Longpre et al. 2025), rather than indicative of fractionation within the plumbing system at depth. This more-evolved carrier melt has been suggested to have been progressively included in the ascending magma due to collapse of mushy feeder structures (Scarrow et al., 2024), hence the same causative process that liberated the melt caused the shutdown of the eruption (Fig. 12).

While this 'shutting down' stage is invisible to the macrocryst crystal cargo itself, the compositional uniformity of the crystal cargo is a critical observation. For instance, should the crystal cargo have changed in character, we would need to account for this and potentially suggest different magma sources, or invoke dynamic fractionation during eruption, and then seek to test these hypotheses with thermometry (we would expect a cooling trend of eruptive temperatures) and/or in-situ isotopic work to prove the existence of distinct magma batches. Yet the crystal cargo maintaining its character argues strongly against wholescale change in the nature, origin, or number of magma sources. Instead, its consistency reveals the melt to be the agent causing the change, which explains the more subtle change in whole-rock compositions, and leads to an interpretation that includes direct implications for eruption longevity.

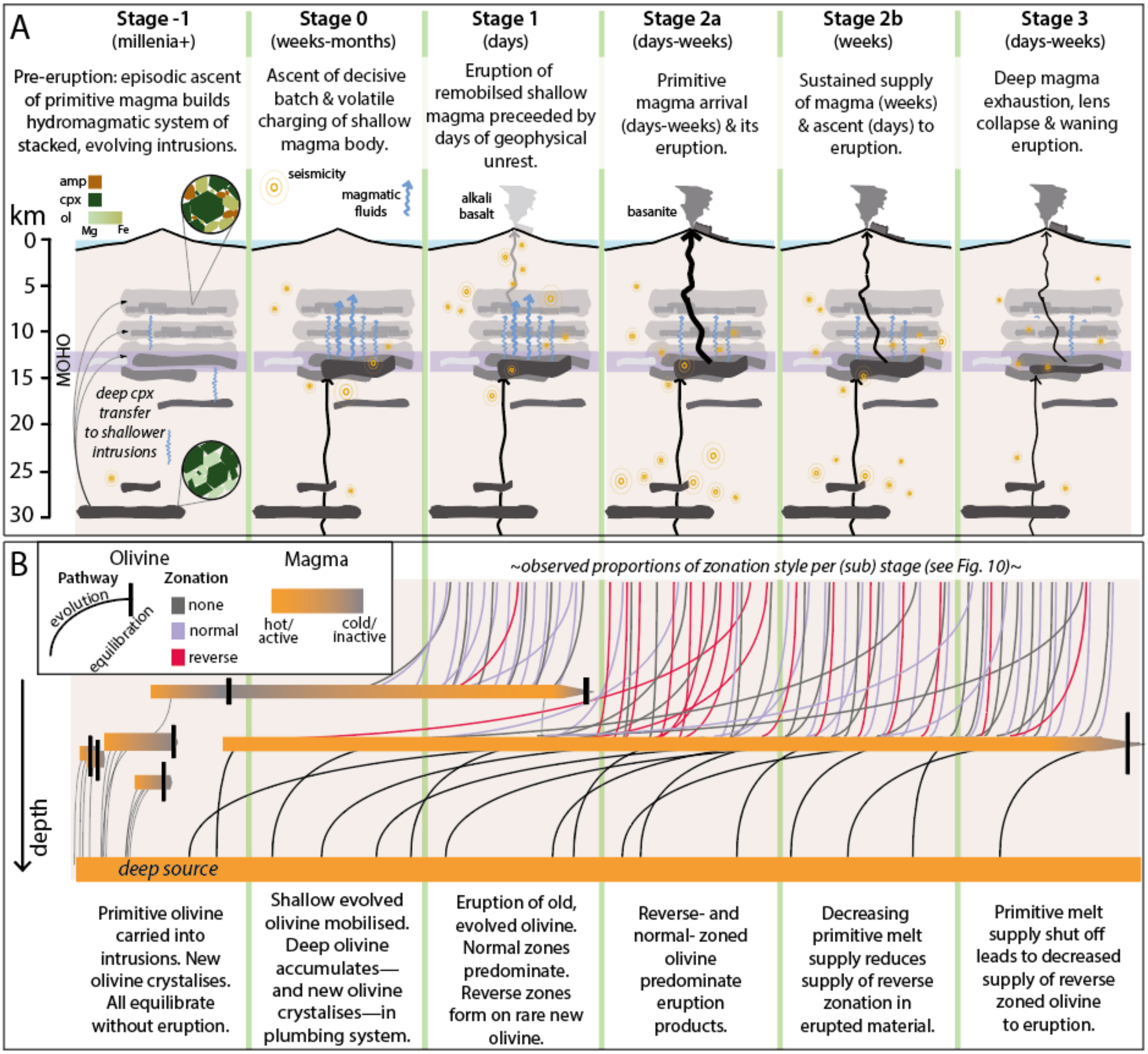

Figure 12: Explanation of olivine zonation populations and diffusion timescale data within the observed eruption phenomenology. Panel A: pre-eruption stages of the plumbing system include intrusion of magma carrying deep clinopyroxene, which evolve by olivine and amphibole crystallization at shallow levels, the latter partly due to continued hydration from deep magmatic fluids (Stage -1). Ascent of the primitive magma batch which exsolves the fluids that finally remobilized old magma (Stage 0) and causes the eruption, which then progresses as characterised by Scarrow et al. (2024) in 3 key stages. Panel B: Schematic olivine pathways through the magmatic system. The first olivine to erupt is dominated by normal- and un-zoned populations. Coupled with the low

abundance and fayalitic composition (Fig. 4) they correspond to the over-pressured hydrated shallow magma body whose eruption defines Stage 1. The primitive magma ascends during stage 1, interacting with more evolved olivine and causing reverse zones, which dominate the olivine zonation populations in Stage 2a. Diffusion timescales demonstrate a weeks-long period of some interaction in an environment not represented in Stage 1, confirming a spatial-temporal disconnect between magma sources. The proportion of reverse zoned olivine decreases through stage 2a and is absent in the last sample analysed in Stage 3, indicating a waning supply of primitive melt through time.

Use of mineralogical information in monitoring eruption progression and cessation

The high temporal resolution of geochemical, geophysical, petrological and physical volcanology data available for the Tajogaite eruption make this event a useful key to consider what information can be used most effectively to forecast onset, progression and cessation of future eruptions. Mineralogical data can be more costly to obtain than whole-rock or glass data, and can often require more sample processing (and time) prior to analysis (Re et al., 2021). However, information about the complexity of magma stalling and ascent pathways are generally only possible from recovering crystal scale histories (e.g. Kahl et al., 2021; Halldórsson et al., 2022; Weber et al., 2023; Chamberlain et al., 2024). Advances in workflows and methods can allow geochemical data on eruptive products to be obtained much more rapidly and in recent years near real-time analyses of whole-rock samples and glass have been used to understand eruption progression (e.g. Gansecki et al., 2021; Corsaro & Miraglia, 2022; Pankhurst et al., 2022). Therefore, using mineral-scale information to aid in interpreting whole-rock or melt composition changes are key.

The most important question petrographic study can help to address is how an eruption might evolve and especially when an eruption will end. Scarrow et al (2024) highlight the importance of the Stage 2 – Stage 3 transition as marking the onset of eruption cessation. Additionally, they noted that changes in Tajogaite whole-rock compositions shared similar trends to those observed to precede the cessation of the 2018 Kīlauea and 2021 Fagradalsfjall eruptions, where all three events erupted slightly more-evolved material in the final few weeks of activity (Gansecki et al., 2019; Bindeman et al., 2022; Halldórsson et al., 2022; Day et al., 2022; Scarrow et al., 2024). Yet, being able to link these changes in whole-rock compositions to specific magmatic processes and shutdown of the eruption requires comparison with the mineralogical record, to assess whether the changes reflect varying degrees of crystal incorporation, varying compositions of mineralogical cargo, or whether the melt composition is changing. Importantly, the macrocryst crystal data collected here, coupled with whole-rock and melt data, show that the mineral cargo (both composition and abundance) does not change at the Stage 2 to Stage 3 transition, therefore suggesting that the feeder system is starting to withdraw remnant melt due to decreased magma flux and related collapse of the magmatic system (Fig. 12; Scarrow et al., 2024; Longpré et al., 2025).

In eruptions where the crystal cargo is more dominant and/or more variable, obtaining a reliable melt signature could be more challenging. At Tajogaite the simultaneous and near-continuous eruption of both lava and tephra provided the opportunity to analyse both the melt (tephra glass) without the complications of post-eruption crystallisation, and the magma (lava) without the complications of post-eruption winnowing. The resulting data streams offered intercomparison for the entire duration of the eruption and provided the opportunity to spot covarying and non-co-varying trends, which led to the insights published so far, yet this situation is a rarity in the rock record. These considerations highlight the importance of initial detailed study of erupted products before deciding on the analytical approach for petrological monitoring, and as emphasised by Re et al., (2021) and Scarrow et al. (2024)- preparedness in terms of workflows and laboratory agreements are vital to embed petrological monitoring into eruption response methodologies (cf., Gansecki et al., 2019).

Use of mineralogical information in interpreting past eruptions

By undertaking daily collection of tephra and near-daily collection of lavas in the 2021 Tajogaite eruption, we can interrogate the petrologic record of the eruption and record a time-series evolution of the magma feeding the Tajogaite eruption. In contrast to this approach, sampling of older eruptions is often much more limited than the sampling of recent eruptions, as in many cases the sequence of lava emplacement may be unknown and the temporal relationships between lava and tephra products may not be preserved, at least without some ambiguity. Additionally, financial and/or logistical restrictions may limit the number of samples collected and investigated for a single eruptive sequence. Yet many volcanoes have no historically recorded eruptions, and thus only pre-historic eruptions are available to understand the magmatic plumbing system and eruption progression processes.

How an eruption begins, and what triggers the eruption to begin are key questions in forecasting future eruptive events, yet the mineralogical information presented here highlight that the earliest erupted material does not record a clear or classic trigger and instead shows slightly more-evolved, more diverse and potentially remanent magma being mobilised in the earliest stages of the eruption. The ascent and intrusion of fresher, more primitive magmas (that are likely to have triggered the eruption) are only evident in Stage 2 onwards, with the increased presence of olivine macrocrysts (Fig. 4) which show a rapid change to dominantly reverse-zoned textures (Fig. 10).

If eruptive product samples from the first ~5 days had not been collected, we may interpret that the intrusion of less-evolved melt interacted directly with stagnant melts, and triggered the eruption. Instead, it appears that a more complex process, where intrusions of more primitive magmas began at least a few weeks before the eruption commenced (Fig. 11) and eventually allowed stagnant, more-evolved melts to be erupted, which requires a distinctly different trigger mechanism/s or response timescale such as fluxing of volatiles or changing crustal stress states (Caricchi et al., 2021). Often, the very earliest erupted material is immediately covered by subsequent eruptive outputs- indeed the earliest lava sample sites at Tajogaite are now buried beneath later effusions (Fig. 1). It is therefore likely that other prehistoric eruptions which do not have the very earliest erupted material preserved or accessible lack the resolution to identify the multi-stage processes responsible for eruption triggering.

Of near equal importance for managing volcanic crises, is understanding how and when an eruption will end; and yet the mineralogical data presented here record no direct evidence for magmatic shutdown (i.e. Stage 2 to Stage 3 boundary). However, identification of transitions to more-evolved whole-rock and melt compositions in the final few days-weeks of multiple historic eruptions (Scarrow et al., 2024) suggests that there are some similar processes occurring (at least in long-lived mafic ocean island eruptions). The identification of this Stage 3 phase at Tajogaite highlights the importance of collecting samples throughout eruptive sequences to understand how magmatic processes and the tapping of different magmas progresses with time.

The identification of discrete phases within long-lived mafic eruptions underscores the importance of careful sampling when studying past eruptions that lack a detailed timeline. Detailed field assessments of the relative timing of samples compared with the range of products from the eruption should be undertaken prior to petrological study. In addition, rapid whole-rock analyses could be carried out to allow future investigators to carefully target advanced mineralogical study on representative samples. In parallel, rapid automated mineralogy techniques (e.g. QEMSCAN®), tuned for application to volcanological products, would provide the complementary data needed to deconvolve the role of crystals and melt in defining the whole-rock composition, and reconcile the signals seen from rapid whole-rock analyses with subvolcanic processes. Ultimately, detailed and thorough study of recent (and well-instrumented) eruptions (alongside future eruptions) will provide the key to interpret the geological record of eruptions, and improve forecasting of future eruption onset, evolution, and cessation.

Conclusions

In this contribution we have integrated a time series of mineralogical data with existing whole-rock compositional data (Day et al., 2022, Ubide et al., 2023, Scarrow et al., 2024) and compared against timescales of geophysical monitoring data (Civico et al., 2022; D'Auria et al., 2022; Romero et al., 2022, Fabbrizio et al., 2023) to understand how the 2021 Tajogaite eruption progressed, with implications for future monitoring of long-lived eruptive events:

1. Measured mineral proportions and compositions are remarkably uniform throughout the 2021 Tajogaite eruptive sequence and important subtle changes could be easily missed without high-frequency sampling. The presence, then absence, of amphibole and changes in olivine (textures, abundance and compositions) are identified at the transition from Stage 1 to Stage 2 of the eruption (over approximately days 5-10), which is interpreted to reflect progressive tapping of more mafic melts that have experienced mixing in the days to weeks prior to eruption onset. Extended application of diffusion chronometry from the Tajogaite crystal record will allow these timescales to be verified and expanded upon.

2. Modelled growth conditions (pressures and temperatures) of clinopyroxene, the dominant macrocryst phase in the 2021 eruption, demonstrate that there is no systematic difference in the depths over which magmas were sourced during the eruption. Calculated pressures of ~800 MPa are in agreement with a deeper (~27 km depth) storage zone in the upper mantle identified from past barometry and geophysical observations of sources of seismicity (see Scarrow et al., 2024 for summary). No mineralogical evidence is found for the previously identified shallower zone of magma storage at ~6–16 km from both seismic, and melt and fluid inclusion studies (D'Auria et al., 2022; Sandoval-Velasquez et al., 2023; Zanon et al., 2024) of the Tajogaite eruption.
3. No mineralogical changes are observed at the transition from Stage 2 (eruption progression) and Stage 3 (cessation), which was identified from whole-rock and glass analyses (Longpré et al., 2025; Scarrow et al., 2024). Hence the variation in whole-rock chemistry (as reported by Scarrow et al., 2024) is solely a function of changing melt compositions. This observation supports the model of Scarrow et al (2024) where compaction and collapse of magma storage regions extracts more-evolved melt compositions when the magma supply from depth wanes (Fig. 12), ultimately leading to the end of the eruption.
4. The identification of the transition to Stage 3 at Tajogaite, and the recognition of similar changes in other recent eruptions (Scarrow et al., 2024) highlights the importance of petrological monitoring in forecasting eruption progression and cessation (e.g. Gansecki et al., 2019, Re et al., 2021, Bindeman et al., 2022; Halldórsson et al., 2022). The mineralogical data collected here highlights that, in fact, whole-rock analyses (chemical and textural) should be the priority when considering which techniques to use in forecasting of eruptive activity in mafic ocean island eruptions. However, further work is needed in more diverse magmatic systems where assembly and evolution of magmas may be more complex than recent eruptions from La Palma, Iceland and Hawai'i.

Author contributions

KJC, MJP, JHS, DAN, DJM, OAB, JH conceived of the project and secured funding for the study. Samples were collected by MJP, BCC, JHS, OAB, JH, KJC, AGS, AM-L and FR. MJP, DAN, DJM, SB-

F, JG, GKR, PEW, AGS contributed to collecting data and modelling results presented here. KJC wrote the manuscript with support from MJP and DAN. All authors provided critical feedback and helped shape the manuscript.

Acknowledgements

The authors are grateful to reviewers Geoff Kilgour and Teresa Ubide for their carefully considered comments, and to editor Sami Mikhail for handling of this manuscript. This study was made possible by financial support from Natural Environment Research Council (NERC) Urgency grant number: NE/W007673/1. DAN acknowledges support from NERC (NE/T011106/1)

The authors gratefully acknowledge extensive support in the field, including that from: Antonio Álvarez, Alexander G. Stewart, Alba Martín-Lorenzo, Charline Lormand, David Calvo Fernández, Eillish Brennan, Ella Curtis, Ed Llewellin, Eleazar Padrón, Germán Padilla-Hernández, Germán Cervigón Tomico, Guillermo Recio Sotelo, Ivan Cabrera-Perez, José Barrancos, Jorge Romero, María Asensio Ramos, Pedro Hernández, Rachel Bilsland, Ulrich Keuppers, Victor Ortega Ramos, Nemesio Pérez, William Hernández and Rebecca Winstanley. Finally, the authors express their thanks to David Olivier for rock preparation and additional lab assistance at the University of Manchester.

Data availability

All data is available as supplementary appendices linked to this manuscript. Datasets are available on the National Geoscience Data Centre: http://data.bgs.ac.uk/id/dataHolding/13608248; http://data.bgs.ac.uk/id/dataHolding/13608284.

References

Allan, A. S., Morgan, D. J., Wilson, C. J., & Millet, M. A. (2013). From mush to eruption in centuries: assembly of the super-sized Oruanui magma body. *Contributions to Mineralogy and Petrology*, *166*, 143-164. https://doi.org/10.1007/s00410-013-0869-2

Barker, A. K., Troll, V. R., Carracedo, J. C., & Nicholls, P. A. (2015). The magma plumbing system for the 1971 Teneguía eruption on La Palma, Canary Islands. *Contributions to Mineralogy and Petrology*, *170*, 1-21.https://doi.org/10.1007/s00410-015-1207-7

Bell, S. K., Morgan, D. J., Joy, K. H., Pernet-Fisher, J. F., & Hartley, M. E. (2023). Determining the thermal histories of Apollo 15 mare basalts using diffusion modelling in olivine. *Geochimica et Cosmochimica Acta*, *357*, 77-91 .https://doi.org/10.1016/j.gca.2023.08.009

Bernard, B., Stock, M. J., Coppola, D., Hidalgo, S., Bagnardi, M., Gibson, S., ... & Gleeson, M. (2019). Chronology and phenomenology of the 1982 and 2015 Wolf volcano eruptions, Galápagos Archipelago. *Journal of Volcanology and Geothermal Research*, *374*, 26-38. https://doi.org/10.1016/j.jvolgeores.2019.02.013

Bindeman, I. N., Deegan, F. M., Troll, V. R., Thordarson, T., Höskuldsson, Á., Moreland, W. M., ... & Walter, T. R. (2022). Diverse mantle components with invariant oxygen isotopes in the 2021 Fagradalsfjall eruption, Iceland. *Nature Communications*, *13*(1), 3737.https://doi.org/10.1038/s41467-022-31348-7

Bonadonna, C., Pistolesi, M., Biass, S., Voloschina, M., Romero, J., Coppola, D., ... & Rodríguez, F. (2022). Physical characterization of long-lasting hybrid eruptions: the 2021 Tajogaite eruption of Cumbre Vieja (La Palma, Canary Islands). *Journal of Geophysical Research: Solid Earth*, *127*(11), e2022JB025302.https://doi.org/10.1029/2022JB025302

Bonechi, B., Polacci, M., Arzilli, F., Romero, J., Fellowes, J., & Burton, M. (2024). Magma residence time, ascent rate and eruptive style of the November ash-laden activity during the 2021 Tajogaite eruption (La Palma, Spain). *Volcanica*, *7*(1), 51-65. https://doi.org/10.30909/vol.07.01.5165

Caricchi, L., Townsend, M., Rivalta, E., & Namiki, A. (2021). The build-up and triggers of volcanic eruptions. *Nature Reviews Earth & Environment*, *2*(7), 458-476. https://doi.org/10.1038/s43017-021-00174-8

Carracedo, J. C. (1994). The Canary Islands: an example of structural control on the growth of large oceanic-island volcanoes. *Journal of Volcanology and Geothermal Research*, *60*(3-4), 225-241. https://doi.org/10.1016/0377-0273(94)90053-1

Carracedo, J. C., Day, S., Guillou, H., Badiola, E. R., Cañas, J. A., & Torrado, F. P. (1998). Hotspot volcanism close to a passive continental margin: the Canary Islands. *Geological magazine*, *135*(5), 591-604. doi:10.1017/S0016756898001447

Carracedo, J. C., Day, S. J., Guillou, H., & Gravestock, P. (1999). Later stages of volcanic evolution of La Palma, Canary Islands: Rift evolution, giant landslides, and the genesis of the Caldera de Taburiente. *Geological Society of America Bulletin*, *111*(5), 755-768. https://doi.org/10.1130/0016-7606(1999)111<0755:LSOVEO>2.3.CO;2

Carracedo, J. C., Badiola, E. R., Guillou, H., de La Nuez, J., & Torrado, F. P. (2001). Geology and volcanology of la Palma and el Hierro, western Canaries. *Estudios Geologicos-Madrid*, *57*, 175-273.

Carracedo, J. C., Troll, V. R., Day, J. M., Geiger, H., Aulinas, M., Soler, V., ... & Albert, H. (2022). The 2021 eruption of the Cumbre Vieja volcanic ridge on La Palma, canary islands. *Geology Today*, *38*(3), 94-107. https://doi.org/10.1111/gto.12388

Cassidy, M., Manga, M., Cashman, K., & Bachmann, O. (2018). Controls on explosive-effusive volcanic eruption styles. *Nature communications*, *9*(1), 2839. https://doi.org/10.1038/s41467-018-05293-3

Chamberlain, K. J., Morgan, D. J., & Wilson, C. J. (2014). Timescales of mixing and mobilisation in the Bishop Tuff magma body: perspectives from diffusion chronometry. *Contributions to Mineralogy and Petrology*, *168*, 1-24. https://doi.org/10.1007/s00410-014-1034-2

Chamberlain, K. J., Morgan, D. J., Lara, L. E., Walshaw, R., Gardner, J., Chenery, S., ... & Wagner, D. (2024). Effect of crustal stress state on magmatic stalling and ascent: case study from Puyehue-Cordón Caulle, Chile. *Bulletin of Volcanology*, *86*(6), 53. https://doi.org/10.1007/s00445-024-01740-w

Civico, R., Ricci, T., Scarlato, P., Taddeucci, J., Andronico, D., Del Bello, E., ... & Pérez, N. M. (2022). High-resolution digital surface model of the 2021 eruption deposit of Cumbre Vieja volcano, La Palma, Spain. *Scientific Data*, *9*(1), 435. https://doi.org/10.1038/s41597-022-01551-8

Conway, C. E., Chamberlain, K. J., Harigane, Y., Morgan, D. J., & Wilson, C. J. (2020). Rapid assembly of high-Mg andesites and dacites by magma mixing at a continental arc stratovolcano. *Geology*, *48*(10), 1033-1037. https://doi.org/10.1130/G47614.1

Corsaro, R. A., & Miraglia, L. (2022). Near real-time petrologic monitoring on volcanic glass to infer magmatic processes during the February–April 2021 paroxysms of the South-East Crater, Etna. *Frontiers in Earth Science*, *10*, 828026. https://doi.org/10.3389/feart.2022.828026

Couperthwaite, F. K., Thordarson, T., Morgan, D. J., Harvey, J., & Wilson, M. (2020). Diffusion timescales of magmatic processes in the Moinui lava eruption at Mauna Loa, Hawaii, as inferred from bimodal olivine populations. *Journal of Petrology*, *61*(7), egaa058.https://doi.org/10.1093/petrology/egaa058

Couperthwaite, F. K., Morgan, D. J., Pankhurst, M. J., Lee, P. D., & Day, J. M. (2021). Reducing epistemic and model uncertainty in ionic inter-diffusion chronology: a 3D observation and dynamic modeling approach using olivine from Piton de la Fournaise, La Réunion. *American Mineralogist*, *106*(3), 481-494. https://doi.org/10.2138/am-2021-7296CCBY

Couperthwaite, F. K., Morgan, D. J., Harvey, J., & Kahl, M. (2022). Pre-eruptive timescales from the historical Hapaimamo eruption at Mauna Loa, Hawai ‘i. *Journal of Volcanology and Geothermal Research*, *432*, 107690. https://doi.org/10.1016/j.jvolgeores.2022.107690

D’Auria, L., Koulakov, I., Prudencio, J., Cabrera-Pérez, I., Ibáñez, J. M., Barrancos, J., ... & Peréz, N. M. (2022). Rapid magma ascent beneath La Palma revealed by seismic tomography. *Scientific Reports*, *12*(1), 17654. https://doi.org/10.1038/s41598-022-21818-9

Day, S. J., Carracedo, J. C., Guillou, H., & Gravestock, P. (1999). Recent structural evolution of the Cumbre Vieja volcano, La Palma, Canary Islands: volcanic rift zone reconfiguration as a precursor to volcano flank instability?. *Journal of Volcanology and Geothermal Research*, *94*(1-4), 135-167. https://doi.org/10.1016/j.epsl.2022.117793

Day, J. M., Troll, V. R., Aulinas, M., Deegan, F. M., Geiger, H., Carracedo, J. C., ... & Perez-Torrado, F. J. (2022). Mantle source characteristics and magmatic processes during the 2021 La Palma eruption. *Earth and planetary science letters*, *597*, 117793.

Dayton, K., Gazel, E., Wieser, P., Troll, V. R., Carracedo, J. C., La Madrid, H., ... & Perez-Torrado, F. J. (2023). Deep magma storage during the 2021 La Palma eruption. *Science* advances, 9(6), eade7641. DOI: 10.1126/sciadv.ade7641

Dayton, K., Gazel, E., Wieser, P., Troll, V., Carracedo, J., Aulinas, M., & Perez-Torrado, F. (2024). Magmatic storage and volatile fluxes of the 2021 La Palma eruption. *Geochemistry, Geophysics, Geosystems*, *25*(6), e2024GC011491. https://doi.org/10.1029/2024GC011491

Devine, J.D., Rutherford, M. J., Garnder, J.E. (1998). Petrologic determination of ascent rates for the 1995-1997 Soufriere Hills Volcano andesitic magma. Geophysical Research Letters, 25(19) 3673-3676. https://doi.org/10.1029/98GL01330

DeVitre, C. L., Gazel, E., Allison, C. M., Soto, G., Madrigal, P., Alvarado, G. E., & Lücke, O. H. (2019). Multi-stage chaotic magma mixing at Turrialba volcano. *Journal of Volcanology and Geothermal Research*, *381*, 330-346.https://doi.org/10.1016/j.jvolgeores.2019.06.011

Di Fiore, F., Vona, A., Scarani, A., Giordano, G., Romano, C., Giordano, D., ... & Pankhurst, M. (2023). Experimental constraints on the rheology of lavas from 2021 Cumbre Vieja eruption (La Palma, Spain). *Geophysical Research Letters*, *50*(4), e2022GL100970. https://doi.org/10.1029/2022GL100970

Didonna, R., Handley, H., Albert, H., Costa, F. (2024) Time scales of olivine storage and transport as revealed by diffusion chronometry at Waitomokia Volcanic Complex, Auckland Volcanic Field, New Zealand. *Journal of Volcanology and Geothermal Research* 451, 108094. https://doi.org/10.1016/j.jvolgeores.2024.108094

Dimanov, A., & Sautter, V. (2000). "Average" interdiffusion of (Fe, Mn)-Mg in natural diopside. *European Journal of Mineralogy*, *12*(4), 749-760. https://doi.org/10.1127/0935-1221/2000/0012-0749

Dohmen, R., & Chakraborty, S. (2007). Fe–Mg diffusion in olivine II: point defect chemistry, change of diffusion mechanisms and a model for calculation of diffusion coefficients in natural olivine. *Physics and Chemistry of Minerals*, *34*(6), 409-430. https://doi.org/10.1007/s00269-007-0158-6

Fabbrizio, A., Bamber, E. C., Michailidou, E., Romero, J. E., Arzilli, F., Bonechi, B., Polacci, M & Burton, M. (2023). Phase equilibrium experiments and thermodynamic simulations to constrain the pre-eruptive conditions of the 2021 Tajogaite eruption (Cumbre Vieja volcano, La Palma, Canary Islands). *Journal of Volcanology and Geothermal Research*, *442*, 107901.https://doi.org/10.1016/j.jvolgeores.2023.107901

Fernández, J., Escayo, J., Hu, Z., Camacho, A. G., Samsonov, S. V., Prieto, J. F., ... & Ancochea, E. (2021). Detection of volcanic unrest onset in La Palma, Canary Islands, evolution and implications. *Scientific reports*, *11*(1), 2540. https://doi.org/10.1038/s41598-021-82292-3

Frascerra, D., Scaillet, B., Andújar, J., Oppenheimer, C., Scaillet, S., Martí, J., Casillas, R & López, C. (2024). Experimental constraints on the behaviour of sulphur in the 2021 Cumbre Vieja (La

Palma) basanite. *Journal of Volcanology and Geothermal Research*, *456*, 108219. https://doi.org/10.1016/j.jvolgeores.2024.108219.

Gansecki, C., Lee, R. L., Shea, T., Lundblad, S. P., Hon, K., & Parcheta, C. (2019). The tangled tale of Kīlauea's 2018 eruption as told by geochemical monitoring. *Science*, *366*(6470), eaaz0147. DOI: 10.1126/science.aaz0147

Geldmacher, J., Hoernle, K., Bogaard, P. V. D., Duggen, S., & Werner, R. (2005). New 40Ar/39Ar age and geochemical data from seamounts in the Canary and Madeira volcanic provinces: support for the mantle plume hypothesis. *Earth and Planetary Science Letters*, *237*(1-2), 85-101.https://doi.org/10.1016/j.epsl.2005.04.037

González-García, D., Boulesteix, T., Klügel, A., & Holtz, F. (2023). Bubble-enhanced basanite–tephrite mixing in the early stages of the Cumbre Vieja 2021 eruption, La Palma, Canary Islands. *Scientific Reports*, *13*(1), 14839. https://doi.org/10.1038/s41598-023-41595-3

Gottlieb, P., Wilkie, G., Sutherland, D., Ho-Tun, E., Suthers, S., Perera, K., ... & Rayner, J. (2000). Using quantitative electron microscopy for process mineralogy applications. *Jom*, *52*(4), 24-25. https://doi.org/10.1007/s11837-000-0126-9

Halldórsson, S. A., Bali, E., Hartley, M. E., Neave, D. A., Peate, D. W., Guðfinnsson, G. H., ... & Thordarson, T. (2018). Petrology and geochemistry of the 2014–2015 Holuhraun eruption, central Iceland: compositional and mineralogical characteristics, temporal variability and magma storage. *Contributions to Mineralogy and Petrology*, *173*, 1-25. https://doi.org/10.1007/s00410-018-1487-9

Halldórsson, S. A., Marshall, E. W., Caracciolo, A., Matthews, S., Bali, E., Rasmussen, M. B., Ranta, E., Gunnarsson, J. R., Guðfinnsson, G. H., Sigmarsson, O., Maclennan, J., Jackson, M. G., Whitehouse, M. J., Jeon, H., van der Meer, Q. H. A., Mibei, G. K., Kalliokoski, M. H., Repczynska, M. M., Rúnarsdóttir, R. H., Sigurðsson, G., Pfeffer, M. A., Scott, S. W., Kjartansdóttir, R., Kleine, B. I., Oppenheimer, C., Aiuppa, A., Ilyinskaya, E., Bitetto, M., Giudice, G., & Stefánsson, A. (2022). Rapid shifting of a deep magmatic source at Fagradalsfjall volcano, Iceland. *Nature, 609*, 529-534. https://doi.org/10.1038/s41586-022-04981-x

Hammer, J., Jacob, S., Welsch, B., Hellebrand, E., & Sinton, J. (2016). Clinopyroxene in postshield Haleakala ankaramite: 1. Efficacy of thermobarometry. *Contributions to Mineralogy and Petrology*, *171*, 1-23.

Hansteen, T. H., Klügel, A., & Schmincke, H. U. (1998). Multi-stage magma ascent beneath the Canary Islands: evidence from fluid inclusions. *Contributions to Mineralogy and Petrology*, *132*(1), 48-64. https://doi.org/10.1007/s004100050404

Hildner, E., Klügel, A., & Hansteen, T. H. (2012). Barometry of lavas from the 1951 eruption of Fogo, Cape Verde Islands: Implications for historic and prehistoric magma plumbing systems. *Journal of volcanology and geothermal research*, *217*, 73-90. https://doi.org/10.1016/j.jvolgeores.2011.12.014

Hoernle, K. A. J., & Schmincke, H. U. (1993). The petrology of the tholeiites through melilite nephelinites on Gran Canaria, Canary Islands: crystal fractionation, accumulation, and depths of melting. *Journal of Petrology*, *34*(3), 573-597.https://doi.org/10.1093/petrology/34.3.573

Houghton, B. F., Cockshell, W. A., Gregg, C. E., Walker, B. H., Kim, K., Tisdale, C. M., & Yamashita, E. (2021). Land, lava, and disaster create a social dilemma after the 2018 eruption of Kīlauea volcano. *Nature communications*, *12*(1), 1223. https://doi.org/10.1038/s41467-021-21455-2

Kahl, M., Bali, E., Guðfinnsson, G. H., Neave, D. A., Ubide, T., Van Der Meer, Q. H., & Matthews, S. (2021). Conditions and dynamics of magma storage in the Snæfellsnes volcanic zone, Western Iceland: insights from the Búðahraun and Berserkjahraun eruptions. *Journal of Petrology*, *62*(9), egab054. doi: 10.1093/petrology/egab054

Kahl, M., Mutch, E. J. F., Maclennan, J., Morgan, D. J., Couperthwaite, F., Bali, E., ... & Askew, R. A. (2023). Deep magma mobilization years before the 2021 CE Fagradalsfjall eruption, Iceland. *Geology*, *51*(2), 184-188. https://doi.org/10.1130/G50340.1

Klügel, A. (1998). Reactions between mantle xenoliths and host magma beneath La Palma (Canary Islands): constraints on magma ascent rates and crustal reservoirs. *Contrib Mineral Petrol* **131**, 237–257. https://doi.org/10.1007/s004100050391

Klügel, A., Hansteen, T. H., & Galipp, K. (2005). Magma storage and underplating beneath Cumbre Vieja volcano, la Palma (Canary Islands). *Earth and Planetary Science Letters*, *236*(1-2), 211-226. https://doi.org/10.1016/j.epsl.2005.04.006

Leake, B. E., Woolley, A. R., Arps, C. E., Birch, W. D., Gilbert, M. C., Grice, J. D., ... & Youzhi, G. (1997). Nomenclature of amphiboles; report of the Subcommittee on Amphiboles of the International Mineralogical Association Commission on new minerals and mineral names. *Mineralogical magazine*, *61*(405), 295-310. doi:10.1180/minmag.1997.061.405.13

Longpré, M.-A., Tramontano, S., Pankhurst, M.J.,Roman, D.C., Reiss, M.C., Cortese, F., James, M.R., Spina, L., Rodríguez, F., Coldwell, B., Martín-Lorenzo, A. 4,10, Olivia Barbee, O., D'Auria, L., Chamberlain, K.J., Scarrow, J.H. (2025) Shifting melt composition linked to volcanic tremor at Cumbre Vieja volcano. *Nature Geoscience, 18,* 175–183. https://doi.org/10.1038/s41561-024-01623-x

Mangler, M. F., Petrone, C. M., & Prytulak, J. (2022). Magma recharge patterns control eruption styles and magnitudes at Popocatépetl volcano (Mexico). *Geology*, *50*(3), 366-370. https://doi.org/10.1130/G49365.1

MacDonald, A., Ubide, T., Mollo, S., Pontesilli, A., & Masotta, M. (2023). The Influence of Undercooling and Sector Zoning on Clinopyroxene–Melt Equilibrium and Thermobarometry. *Journal of Petrology*, *64*(10), egad074. https://doi.org/10.1093/petrology/egad074

Matthews S. W., Caracciolo, A., Bali, E., Halldórsson, S. A., Sigmarsson, O., Guðfinnsson, G. H., Pedersen G. B. M., Robin J. G., . Marshall E. W., Aden A. A., Gísladóttir B. Y., Bosq C., Auclair D., Merrill H., Levillayer N., Löw N., Rúnarsdóttir R. H., Johnson S. M., Steinþórsson S. & Drouin, V. (2024). A dynamic mid-crustal magma domain revealed by the 2023 to 2024 Sundhnúksgígar eruptions in Iceland. *Science*, *386*(6719), 309-314. DOI: 10.1126/science.adp8778

Meredith, E.S., Jenkins, S.F., Hayes, J.L., Lallemant, D., Deligne, N.I. and Teng, N.R.(2024). Lava flow impacts on the built environment: insights from a new global dataset. *Journal of Applied Volcanology*, *13*(1), p.1. https://doi.org/10.1186/s13617-023-00140-7

Mollo, S., Del Gaudio, P., Ventura, G., Iezzi, G., & Scarlato, P. (2010). Dependence of clinopyroxene composition on cooling rate in basaltic magmas: Implications for thermobarometry. *Lithos*, *118*(3-4), 302-312. https://doi.org/10.1016/j.lithos.2010.05.006

Mollo, S., Putirka, K., Misiti, V., Soligo, M., & Scarlato, P. (2013). A new test for equilibrium based on clinopyroxene–melt pairs: clues on the solidification temperatures of Etnean alkaline melts at post-eruptive conditions. *Chemical Geology*, *352*, 92-100. https://doi.org/10.1016/j.chemgeo.2013.05.026

Morgan, D. J., & Blake, S. (2006). Magmatic residence times of zoned phenocrysts: introduction and application of the binary element diffusion modelling (BEDM) technique. *Contributions to Mineralogy and Petrology*, *151*, 58-70. https://doi.org/10.1007/s00410-005-0045-4

Mourey, A. J., Shea, T., Costa, F., Shiro, B., & Longman, R. J. (2023). Years of magma intrusion primed Kīlauea Volcano (Hawai'i) for the 2018 eruption: evidence from olivine diffusion chronometry and monitoring data. *Bulletin of Volcanology*, *85*(3), 18. https://doi.org/10.1007/s00445-023-01633-4

Neave, D. A., & Putirka, K. D. (2017). A new clinopyroxene-liquid barometer, and implications for magma storage pressures under Icelandic rift zones. *American Mineralogist*, *102*(4), 777-794. https://doi.org/10.2138/am-2017-5968

Neave, D. A., Bali, E., Guðfinnsson, G. H., Halldórsson, S. A., Kahl, M., Schmidt, A. S., & Holtz, F. (2019). Clinopyroxene–liquid equilibria and geothermobarometry in natural and experimental tholeiites: the 2014–2015 Holuhraun eruption, Iceland. *Journal of Petrology*, *60*(8), 1653-1680.https://doi.org/10.1093/petrology/egz042

Neave, D. A., Maclennan, J., Edmonds, M., & Thordarson, T. (2014). Melt mixing causes negative correlation of trace element enrichment and CO_2 content prior to an Icelandic eruption. *Earth and Planetary Science Letters*, *400*, 272-283. https://doi.org/10.1016/j.epsl.2014.05.050

Neave, D. A., Maclennan, J. (2020). Clinopyroxene dissolution records rapid magma ascent. Frontiers in Earth Science, 8. https://doi.org/10.3389/feart.2020.00188

Ostorero, L., Balcone-Boissard, H., Boudon, G., Shapiro, N. M., Belousov, A., Belousova, M., ... & Droznina, S. Y. (2022). Correlated petrology and seismicity indicate rapid magma accumulation prior to eruption of Kizimen volcano, Kamchatka. *Communications Earth & Environment*, *3*(1), 290. https://doi.org/10.1038/s43247-022-00622-3

Padrón, E., Pérez, N. M., Hernández, P. A., Sumino, H., Melián, G. V., Alonso, M., ... & D’Auria, L. (2022). Early precursory changes in the 3He/4He ratio prior to the 2021 Tajogaite eruption at Cumbre Vieja volcano, La Palma, Canary Islands. *Geophysical Research Letters*, *49*(18), e2022GL099992. https://doi.org/10.1029/2022GL099992

Pankhurst, M. J., Scarrow, J. H., Barbee, O. A., Hickey, J., Coldwell, B. C., Rollinson, G. K., ... & Pérez, N. M. (2022). Rapid response petrology for the opening eruptive phase of the 2021 Cumbre Vieja eruption, La Palma, Canary Islands. *Volcanica*, *5*(1), 1-10. https://doi.org/10.30909/vol.05.01.0110

Pankhurst, M. J., Gueninchault, N., Andrew, M., & Hill, E. (2019). Non-destructive three-dimensional crystallographic orientation analysis of olivine using laboratory diffraction contrast tomography. *Mineralogical Magazine*, *83*(5), 705–711. doi:10.1180/mgm.2019.51

Pankhurst, M. J., Morgan, D. J., Thordarson, T., & Loughlin, S. C. (2018). Magmatic crystal records in time, space, and process, causatively linked with volcanic unrest. *Earth and Planetary Science Letters*, *493*, 231-241.https://doi.org/10.1016/j.epsl.2018.04.025

Paton, C., Hellstrom, J., Paul, B., Woodhead, J., & Hergt, J. (2011). Iolite: Freeware for the visualisation and processing of mass spectrometric data. *Journal of Analytical Atomic Spectrometry*, *26*(12), 2508-2518. https://doi.org/10.1039/C1JA10172B

Perugini, D., & Perugini, D. (2021). Magma Mixing: The Trigger for Explosive Volcanic Eruptions. *The Mixing of Magmas: Field Evidence, Numerical Models, Experiments*, 135-148. https://doi.org/10.1007/978-3-030-81811-1_10

Piña-Varas, P., Ledo, J., Queralt, P., van Dorth, D. M., Marcuello, A., Cabrera-Pérez, I., ... & Martí, A. (2023). Volcanic monitoring of the 2021 La Palma eruption using long-period magnetotelluric data. *Scientific Reports*, *13*(1), 15929. https://doi.org/10.1038/s41598-023-43326-0

Pirrie, D., & Rollinson, G. K. (2011). Unlocking the applications of automated mineral analysis. *Geology Today*, *27*(6), 226-235. https://doi.org/10.1111/j.1365-2451.2011.00818.x

Pizarro, C., Parada, M. A., Contreras, C., & Morgado, E. (2019). Cryptic magma recharge associated with the most voluminous 20th century eruptions (1921, 1948 and 1971) at Villarrica Volcano. *Journal of Volcanology and Geothermal Research*, *384*, 48-63. https://doi.org/10.1016/j.jvolgeores.2019.07.001

Poland, M. P., Miklius, A., & Montgomery-Brown, E. K. (2014). *Magma supply, storage, and transport at shield-stage Hawaiian volcanoes* (No. 1801-5, pp. 179-234). US Geological Survey. http://dx.doi.org/10.3133/pp1801.

Prægel, N. O., & Holm, P. M. (2006). Lithospheric contributions to high-MgO basanites from the Cumbre Vieja Volcano, La Palma, Canary Islands and evidence for temporal variation in plume influence. *Journal of Volcanology and Geothermal Research*, *149*(3-4), 213-239. https://doi.org/10.1016/j.jvolgeores.2005.07.019

Putirka, K. D. (2008). Thermometers and barometers for volcanic systems. *Reviews in mineralogy and geochemistry*, *69*(1), 61-120. https://doi.org/10.2138/rmg.2008.69.3

Putirka, K., Johnson, M., Kinzler, R., Longhi, J., & Walker, D. (1996). Thermobarometry of mafic igneous rocks based on clinopyroxene-liquid equilibria, 0–30 kbar. *Contributions to Mineralogy and Petrology*, *123*, 92-108. https://doi.org/10.1007/s004100050145

Re, G., Corsaro, R. A., D'Oriano, C., & Pompilio, M. (2021). Petrological monitoring of active volcanoes: A review of existing procedures to achieve best practices and operative protocols during eruptions. *Journal of Volcanology and Geothermal Research*, *419*, 107365. https://doi.org/10.1016/j.jvolgeores.2021.107365

Ridolfi, F., & Renzulli, A. (2012). Calcic amphiboles in calc-alkaline and alkaline magmas: thermobarometric and chemometric empirical equations valid up to 1,130° C and 2.2 GPa. *Contributions to Mineralogy and Petrology*, *163*, 877-895. https://doi.org/10.1007/s00410-011-0704-6

Rollinson, G. K., Andersen, J. C., Stickland, R. J., Boni, M., & Fairhurst, R. (2011). Characterisation of non-sulphide zinc deposits using QEMSCAN®. *Minerals Engineering*, *24*(8), 778-787. https://doi.org/10.1016/j.mineng.2011.02.004

Romero, J. E., Burton, M., Cáceres, F., Taddeucci, J., Civico, R., Ricci, T., ... & Perez, N. M. (2022). The initial phase of the 2021 Cumbre Vieja ridge eruption (Canary Islands): Products and dynamics controlling edifice growth and collapse. *Journal of Volcanology and Geothermal Research*, *431*, 107642. https://doi.org/10.1016/j.jvolgeores.2022.107642

Ruth, D. C. S., & Costa, F. (2021). A petrological and conceptual model of Mayon volcano (Philippines) as an example of an open-vent volcano. *Bulletin of Volcanology*, *83*(10), 62. https://doi.org/10.1007/s00445-021-01486-9

Sandoval-Velasquez, A., Rizzo, A. L., Casetta, F., Ntaflos, T., Aiuppa, A., Alonso, M., ... & Perez, N. M. (2023). The noble gas signature of the 2021 Tajogaite eruption (La Palma, Canary Islands). *Journal* *of Volcanology and Geothermal Research*, *443*, 107928. https://doi.org/10.1016/j.jvolgeores.2023.107928

Scarrow, J.H., Pankhurst, M.J., Barbee, O.A., Chamberlain, K.J., Morgan, D.J., Longpré, M-A., Tramontano, S., James Hickey, J., Neave, D.A., Rollinson, G.K., Stewart, A.G., Wieser, P.E., Coldwell, B.C, Hernández. W, D'Auria, L.D. & Pérez, N.M. (2024). Decoding links between magmatic processes and eruption dynamics: insights into hindcasting the end of the Tajogaite 2021 eruption, La Palma, from petrological records. *Volcanica, 7(2),* 953-980. https://doi.org/10.30909/vol.07.02.953980

Schmincke, H. U., Klügel, A., Hansteen, T. H., Hoernle, K., & van den Bogaard, P. (1998). Samples from the Jurassic ocean crust beneath Gran Canaria, La Palma and Lanzarote (Canary Islands). *Earth and Planetary Science Letters*, *163*(1-4), 343-360. https://doi.org/10.1016/S0012-821X(98)00168-X

Sides, I., Edmonds, M., Maclennan, J., Houghton, B. F., Swanson, D. A., & Steele-MacInnis, M. J. (2014). Magma mixing and high fountaining during the 1959 Kīlauea Iki eruption, Hawai 'i. *Earth and Planetary Science Letters*, *400*, 102-112. https://doi.org/10.1016/j.epsl.2014.05.024

Soldati, A., Cimarelli, C., Kueppers, U., Cáceres, F., Müller, D., Pankhurst, M., ... & Dingwell, D. B. (2024). Melt viscosity tracks the volcanic and magmatic evolution of the 2021 Tajogaite eruption, La Palma (Canary Islands). *Journal of Volcanology and Geothermal Research*, 108210. https://doi.org/10.1016/j.jvolgeores.2024.108210

Staudigel, H., Feraud, G., & Giannerini, G. (1986). The history of intrusive activity on the island of La Palma (Canary Islands). *Journal of Volcanology and Geothermal Research*, *27*(3-4), 299-322. https://doi.org/10.1016/0377-0273(86)90018-1

Suarez, E. D., Domínguez-Cerdeña, I., Villaseñor, A., Aparicio, S. S. M., del Fresno, C., & García-Cañada, L. (2023). Unveiling the pre-eruptive seismic series of the La Palma 2021 eruption: Insights through a fully automated analysis. *Journal of Volcanology and Geothermal Research*, *444*, 107946. https://doi.org/10.1016/j.jvolgeores.2023.107946

Taddeucci, J., Scarlato, P., Andronico, D., Ricci, T., Civico, R., Del Bello, E., ... & Pérez, N. M. (2023). The explosive activity of the 2021 tajogaite eruption (La Palma, canary islands, Spain).

Geochemistry, Geophysics, Geosystems, *24*(6), e2023GC010946. https://doi.org/10.1029/2023GC010946

Thomson, A., & Maclennan, J. (2013). The distribution of olivine compositions in Icelandic basalts and picrites. *Journal of Petrology*, *54*(4), 745-768. https://doi.org/10.1093/petrology/egs083

Thordarson, T., & Larsen, G. (2007). Volcanism in Iceland in historical time: Volcano types, eruption styles and eruptive history. *Journal of Geodynamics*, *43*(1), 118-152. https://doi.org/10.1016/j.jog.2006.09.005

Torres-González, P. A., Luengo-Oroz, N., Lamolda, H., D'Alessandro, W., Albert, H., Iribarren, I., ... & Soler, V. (2020). Unrest signals after 46 years of quiescence at cumbre vieja, La Palma, Canary Islands. *Journal of Volcanology and Geothermal Research*, *392*, 106757. https://doi.org/10.1016/j.jvolgeores.2019.106757

Troll, V. R., & Carracedo, J. C. (2016). *The geology of the Canary Islands*. Elsevier. ISBN: 9780128096635

Ubide, T., Mollo, S., Zhao, J. X., Nazzari, M., & Scarlato, P. (2019). Sector-zoned clinopyroxene as a recorder of magma history, eruption triggers, and ascent rates. *Geochimica et Cosmochimica Acta*, *251*, 265-283. https://doi.org/10.1016/j.gca.2019.02.021

Ubide, T., Márquez, Á., Ancochea, E., Huertas, M. J., Herrera, R., Coello-Bravo, J. J., ... & Galindo, I. (2023). Discrete magma injections drive the 2021 La Palma eruption. *Science Advances*, *9*(27), eadg4813. DOI: 10.1126/sciadv.adg4813

van Gerve, T. D., Neave, D. A., Wieser, P., Lamadrid, H., Hulsbosch, N., & Namur, O. (2024). The Origin and Differentiation of CO 2-Rich Primary Melts in Ocean Island Volcanoes: Integrating 3D X-Ray Tomography with Chemical Microanalysis of Olivine-Hosted Melt Inclusions from Pico (Azores). *Journal of Petrology*, *65*(2), egae006. https://doi.org/10.1093/petrology/egae006

Wadsworth, F. B., Llewellin, E. W., Farquharson, J. I., Gillies, J. K., Loisel, A., Frey, L., ... & Santabárbara, A. P. (2022). Crowd-sourcing observations of volcanic eruptions during the 2021 Fagradalsfjall and Cumbre Vieja events. *Nature Communications*, *13*(1), 2611. https://doi.org/10.1038/s41467-022-30333-4

Weber, G., Blundy, J., Barclay, J., Pyle, D. M., Cole, P., Frey, H., ... & Cashman, K. (2024). Petrology of the 2020–21 effusive to explosive eruption of La Soufrière Volcano, St Vincent: insights into plumbing system architecture and magma assembly mechanism. *Geological Society, London, Special Publications*, *539*(1), 171-200. https://doi.org/10.1144/SP539-2022-177

Weis, F. A., Skogby, H., Troll, V. R., Deegan, F. M., & Dahren, B. (2015). Magmatic water contents determined through clinopyroxene: Examples from the Western Canary Islands, Spain. *Geochemistry, Geophysics, Geosystems*, *16*(7), 2127-2146. https://doi.org/10.1002/2015GC005800

Wieser, P., Petrelli, M., Lubbers, J., Wieser, E., Özaydin, S., Kent, A. J., & Till, C. (2022). Thermobar: an open-source Python3 tool for thermobarometry and hygrometry. *Volcanica*, 5(2), 349-384. https://doi.org/10.30909/vol.05.02.349384

Wieser, P. E., Kent, A. J., Till, C. B., Donovan, J., Neave, D. A., Blatter, D. L., & Krawczynski, M. J. (2023). Barometers behaving badly I: Assessing the influence of analytical and experimental uncertainty on clinopyroxene thermobarometry calculations at crustal conditions. *Journal of Petrology*, *64*(2), egac126. https://doi.org/10.1093/petrology/egac126

Wieser, P. E., Gleeson, M., Matthews, S., DeVitre, C. L., & Gazel, E. (2025). Determining the Pressure-Temperature-Composition (P-T-X) conditions of magma storage. Invited review chapter, Treatise of Geochemistry. https://doi.org/10.1016/B978-0-323-99762-1.00024-3

Zanon, V., D'Auria, L., Schiavi, F., Cyrzan, K., & Pankhurst, M. J. (2024). Toward a near real-time magma ascent monitoring by combined fluid inclusion barometry and ongoing seismicity. *Science Advances*, *10*(6), eadi4300. DOI: 10.1126/sciadv.adi4300